



Published in final edited form as:

J Phys Chem B. 2013 December 5; 117(48): 14894–14906. doi:10.1021/jp408440z.

Dynamic Nuclear Polarization of ^{17}O : Direct Polarization

Vladimir K. Michaelis, Björn Corzilius[†], Albert A. Smith[‡], and Robert G. Griffin^{*}

Francis Bitter Magnet Laboratory and Department of Chemistry, Massachusetts Institute of Technology, Cambridge, Massachusetts, 02139, USA

Abstract

Dynamic nuclear polarization of ^{17}O was studied using four different polarizing agents – the biradical TOTAPOL, and the monoradicals trityl and SA-BDPA, as well as a mixture of the latter two. Field profiles, DNP mechanisms and enhancements were measured to better understand and optimize directly polarizing this low-gamma quadrupolar nucleus using both mono- and bi-radical polarizing agents. Enhancements were recorded $< 88\text{ K}$ and were > 100 using the trityl (OX063) radical and < 10 with the other polarizing agents. The $> 10,000$ fold savings in acquisition time enabled a series of biologically relevant small molecules to be studied with small sample sizes and the measurement of various quadrupolar parameters. The results are discussed with comparison to room temperature studies and GIPAW quantum chemical calculations. These experimental results illustrate the strength of high field DNP and the importance of radical selection for studying low-gamma nuclei.

Keywords

DNP; NMR; oxygen-17; radicals; cross-effect; solid-effect

1. Introduction

Over the past few decades a number of new methods and technologies have been developed to boost sensitivity and resolution in solid-state NMR experiments, for example Hartmann-Hahn cross polarization¹, magic-angle spinning (MAS)^{2,3}, innovative methods for decoupling⁴⁻⁷, and high magnetic fields ($\sim 16.4\text{ T}$). These improvements have in turn enabled structural studies of peptides⁸ membrane⁹⁻¹² and amyloid proteins¹³⁻¹⁷ which would not be possible using conventional solution-state NMR or diffraction methods. Thus, it is now routine to examine ^{13}C , ^{15}N and ^{31}P spectra, and, to measure distances and torsion angles that lead to molecular structures. More recently the ability to extensively ^2H label proteins together with back exchange of the amide NH's and the availability of probes that spin at $\omega_r/2\pi \sim 65\text{ kHz}$, have made detection of ^1H MAS spectra possible.¹⁸⁻²¹

In contrast, NMR studies of oxygen, the other copious element in biological systems, has progressed slowly due to its low natural abundance (0.037%) and small gyromagnetic ratio ($-5.774 \times 10^7\text{ MHz T}^{-1}$) which leads to inherently low sensitivity. In particular, these two

^{*}Corresponding Author: Robert G. Griffin, rgg@mit.edu.

[†]Current Address: Institute of Physical and Theoretical Chemistry and Center of Biomolecular Magnetic Resonance, Goethe University Frankfurt, Max-von-Laue-Str. 7, 60438 Frankfurt, Germany

[‡]Current Address: Department of Chemistry and Applied Biosciences, Laboratory of Physical Chemistry, ETH-Zürich, CH-8093 Zürich, Switzerland

Associated Content

Supporting Information: GIPAW calculations, high field ^{17}O NMR, MAS DNP NMR, variable field MAS NMR simulations, Tables S1–S3 and Figures S1–S6. This material is available free of charge via the Internet at <http://pubs.acs.org>.

factors result in a sensitivity reduction of ~ 15 when compared to ^{13}C .²² In addition, ^{17}O is a quadrupolar nucleus ($I=5/2$, $Q = -2.558 \text{ fm}^2$) and the spectra exhibit a significant broadening due to the interaction between the quadrupole moment and the asymmetric electric field gradient in the chemical environments in proteins and nucleic acids.²³ Despite these technical difficulties ^{17}O is an appealing species to study since, like nitrogen, it is directly involved in hydrogen bonds, and therefore the chemical shifts are exquisitely sensitive to the chemical environment.^{24–26} Furthermore, also like nitrogen, it possesses a large chemical shift range (~ 1000 ppm), and in addition an interesting quadrupolar interaction.^{27, 28} It is therefore important to develop the spectroscopic techniques that allow observation of ^{17}O with high sensitivity.

In the past, modest sensitivity gains for studying ^{17}O NMR were achieved by using isotopic enrichment and applying population transfer techniques.^{29, 30} It is also possible to remove the 2nd order quadrupolar interaction in order to obtain simplified isotropic spectra. This requires advanced techniques including special instrumentation, for example double rotation (DOR) and dynamic-angle spinning (DAS)^{31, 32}, or special spectroscopic techniques such as multiple-quantum magic angle spinning (MQMAS)³³ and satellite-transition magic angle spinning (STMAS)³⁴. However, when the quadrupole coupling is large (> 5 MHz), as is often found for oxygen environments in proteins and nucleic acids, the excitation efficiency of these approaches drops dramatically; in the case of MQMAS spectra to about $\sim 5\%$.^{35, 36} Thus, although there are a number of exciting MQMAS studies of ^{17}O labeled biological samples, the experimental results are clearly limited by signal-to-noise, hence requiring long acquisition times.^{37–46}

Dynamic nuclear polarization (DNP) has been shown to provide immense gains in NMR sensitivity.^{47–50} This is accomplished by transferring the large electron spin polarization of unpaired electrons to nuclei via microwave irradiation of the electron-nuclear transitions. For efficient DNP, samples are cooled to cryogenic temperatures (< 110 K) where increased electron and nuclear spin-lattice relaxation times (T_{11}) can assist in a more efficient electron-nuclear spin transfer mechanism. For several compelling reasons including reduced ^1H spin-lattice relaxation, improved sensitivity from employing cross polarizing and a large database of nitroxide radicals, optimal for ^1H CE, ^1H is often the nucleus of choice for polarization at cryogenic temperatures using a biradical polarizing agent such as TOTAPOL⁵¹, or other TEMPO biradical variants.^{52–56} Subsequent to polarization of ^1H , a cross-polarization step is used to observe other low-gamma nuclei (e.g., ^{13}C , ^{15}N , etc.).^{47, 49, 57–61} This method (i.e., indirect polarization, $e^- \rightarrow ^1\text{H} \rightarrow \text{X}$, where X is an NMR active nucleus, such as ^{13}C , ^{15}N , ^{17}O , ^{31}P , etc.) has been successfully applied to membrane proteins, peptides, amyloid fibrils, pharmaceuticals, and surfaces, resulting in an enhancement of NMR signal intensity (ϵ) between 30- and 180-fold.^{9, 47, 49, 57, 58, 62–76} Many of these studies focused on $I=1/2$ nuclei (e.g., ^{13}C , ^{31}P , ^{29}Si , etc.) and reports regarding quadrupolar nuclei have been scarce.^{77–81} An alternative to indirect polarization, is polarizing an NMR active nucleus (X) directly from an electron spin source, $e^- \rightarrow \text{X}$, (i.e. direct polarization).^{62, 77, 82–87} This approach is of interest for many chemical systems that cross-polarize by high- γ nuclei (e.g., ^1H or ^{19}F) poorly, found within chemical environments where high- γ nuclei are absent or may be of assistance in spectral editing between protonated and non-protonated chemical environments.

Recently, we illustrated the extension of this approach to ^{17}O using indirect polarization via ^1H DNP.⁷⁸ During that study we determined that the optimized radical for ^1H (i.e., nitroxide-based biradical) performed poorly when polarizing ^{17}O directly.^{88, 89} Similar observations were observed with the biradical bTbk when studying ^{17}O DNP in two synthetic minerals, Periclase (MgO , Cubic-Fm3m) and Brucite ($\text{Mg}(\text{OH})_2$, Trigonal-P3m1).⁸² Herein, we report an extensive study for efficient direct polarization of ^{17}O using a

series of polarizing agents dissolved in a water/glycerol model system. Utilizing enhancements greater than 100, we also show applications of ^{17}O DNP, which are presented in conjunction with quantum chemical calculations – further extending the ability to use DNP to address problems involving low-gamma quadrupolar systems. The reduction in acquisition time for ^{17}O will likely provide a new approach that can be extended to studies in other chemical systems.

2. Theory

2.1. Polarization mechanisms for DNP

Since DNP mechanisms involve the transfer of spin polarization from electrons to nuclei, an exogenous polarizing agent is generally added to the medium containing the solute. Polarizing agents typically are persistent organic mono- or bi-radicals (e.g., trityl (OX063), SA-BDPA, TOTAPOL, etc.), or more recently high-spin metal complexes.⁹⁰ In the case of ^{17}O , a theoretical enhancement of over 4,800, determined by the ratio of the gyromagnetic ratios (i.e., $1_e/1_{17\text{O}}$), is possible.

At high magnetic fields and temperatures close to liquid N_2 there are two dominant mechanisms that mediate electron–nuclear polarization transfer: (1) the cross-effect (CE) and (2) the solid-effect (SE), and both mechanisms require irradiation of the sample with microwaves of appropriate frequency. In the following we will briefly outline the salient features of each.

The cross-effect is a three-spin process between two electrons and a nuclear spin that are dipolar coupled.^{91–96} The difference between the Larmor frequencies of the two electron spins, determined by their g -values and g -anisotropies ($\omega_{0S1}, \omega_{0S2}$) must approximate the nuclear Larmor frequency (ω_{0I}) for maximum efficiency:

$$\omega_{0I} = \left| \omega_{0S1} - \omega_{0S2} \right| \quad (1)$$

For this condition to be met the inhomogeneous breadth (Δ) of the radical's EPR spectrum is required to be larger than the nuclear Larmor frequency, while the homogeneous component (δ) may be smaller than the nuclear Larmor frequency.

$$\Delta > \omega_{0I} > \delta \quad (2)$$

The solid-effect is a two-spin process whereby microwave irradiation is applied at the electron-nuclear zero- or double-quantum frequency.⁹⁷

$$\omega_{mw} = \omega_{0S} \pm \omega_{0I} \quad (3)$$

Due to partial mixing of the nuclear spin states by non-secular electron-nuclear dipolar coupling, these “forbidden” transitions become partially allowed, albeit with a transition moment that is typically 2–3 orders of magnitude smaller than that of the single-quantum EPR transition. Because the zero- and double-quantum transition lead to nuclear enhancements of opposite signs, the homogeneous (δ) and inhomogeneous (Δ) EPR linewidths have to be smaller than the Larmor frequency of the nucleus to be polarized in order to avoid overlap and therefore cancellation of positive and negative enhancements:

$$\omega_{0I} > \delta, \Delta \quad (4)$$

Therefore the SE is the dominant mechanism when polarizing agents with narrow linewidths relative to the nuclear Larmor frequency are used.

2.2. NMR parameters

Since ^{17}O is a quadrupolar nucleus, a coupling between the inherent quadrupole moment and the electric field gradient generated by its surroundings results in a quadrupolar interaction. This coupling will manifest in the observed spectrum and be accompanied by a characteristic shape based on the local symmetry at the ^{17}O site. In solids such as the case for ^{17}O , *vide infra*, the magnetic field Zeeman Field, B_0) is significantly larger than the quadrupolar interaction. This condition allows us to treat the interaction as a perturbation on B_0 , where only the first- and second-order quadrupole interactions are of concern. Hence, the spectra in solids of half-integer quadrupolar nuclei exhibit are governed by the quadrupole Hamiltonian

$$\hat{H}_Q = \sum_k \mathbf{I}_k \mathbf{Q}_k \mathbf{I}_k \quad (5)$$

where the quadrupole coupling tensor \mathbf{Q}_k may be expressed in terms of the electric field gradient tensor \mathbf{V}_k at the k th nuclear site

$$\mathbf{Q}_k = \frac{eQ_k}{2I_k(2I_k - 1)\hbar} \mathbf{V}_k. \quad (6)$$

Here \hat{I} is the nuclear spin operator, \mathbf{V} is the electric field gradient at the quadrupolar nucleus, e is the electric charge, \hbar is defined as usual, and Q_k is the quadrupole moment. Taking $V_{k,zz} = eq_k$ we obtain an expression for the first order frequency

$$\omega_{Qk}^{(1)} = \frac{3e^2q_kQ_k}{4I_k(2I_k - 1)\hbar} \quad (7)$$

The asymmetry is conventionally defined as $\eta_k = (V_{k,xx} - V_{k,yy})/V_{k,zz}$ and leads to the form for the Hamiltonian in the principal axis system where \mathbf{V} is diagonal with components $|V_{zz}|$, $|V_{yy}|$, $|V_{xx}|$.

$$\hat{H}_{Qk} = \omega_{Qk} \left\{ \left(I_{kz}^2 - \frac{1}{3} I_k^2 \right) + \frac{\eta}{3} \left(I_{kx}^2 - I_{ky}^2 \right) \right\} \quad (8)$$

Although the central transition ($m_I = -1/2 \leftrightarrow +1/2$) is not affected by the first-order quadrupole interaction ($\omega_{Qk}^{(1)}$), its lineshape is influenced by a second-order interaction ($\omega_{Qk}^{(2)}$) that scales quadratically with the magnitude of the first-order interaction and inversely with the nuclear Zeeman frequency (ω_{0I})⁹⁷⁻⁹⁹: $\omega_{Qk}^{(2)} = (\omega_{Qk}^{(1)})^2 / \omega_{0I}$

The nuclear quadrupole interaction is described by a coupling constant, C_Q , $C_{Qk} = (eQV_{zzk} / \hbar)$ that typically ranges between 0 and 12 MHz for ^{17}O and an asymmetry parameter, η , which can assume values between 0 and 1.^{28, 100-102} A more comprehensive explanation of the quadrupolar interaction for solids can be found elsewhere.^{98, 103-105}

The chemical shift anisotropy can also influence the appearance of the spectrum, especially under non-spinning conditions and at higher magnetic fields for powdered samples. Although its magnitude is negligible relative to the quadrupole broadening at 5 T for the ^{17}O environments studied here, these parameters should be considered when analyzing higher field spectra.

3. Materials and Methods

3.1. Sample preparation

Samples were prepared using mixtures of *d*₈-glycerol (60 vol. %), D₂O (30 vol. %) and H₂O (10 vol. %). The H₂O was labeled with oxygen-17 (H₂ ¹⁷O – 35%) and was purchased from Cambridge Isotope Laboratories (Andover, MA). Each sample contained 40 mM electron spins homogeneously dispersed at 298 K. The liquid samples were packed into 4 mm o.d. sapphire rotors using between 40 and 60 μL of sample. Samples were prepared with radical concentrations of 20 mM in the case of TOTAPOL and 40 mM of trityl (OX063) and SA-BDPA, respectively. Additionally, an equimolar mixture (i.e., 20 mM trityl and 20 mM SA-BDPA) was prepared. For the experiments shown in section 4.5, 40 mM trityl was dissolved together with ¹³C- ¹⁷O-urea¹⁰⁶ (~20% ¹⁷O) or ¹⁷O-phenol (~30% ¹⁷O) purchased from Cambridge Isotope Laboratories (Andover, MA) with a concentration of 2.0 and 0.65 M, respectively in a mixture of *d*₈-glycerol/D₂O/H₂O (60/30/10 vol.-%), where H₂O was used in natural abundance (0.037%). A third sample containing 40 mM trityl was prepared following the protocol at the beginning of the section to allow for H₂ ¹⁷O NMR analysis. Field profiles were acquired using a mixture of 60/40 (v/v) *d*₈-glycerol/H₂ ¹⁷O (35% - ¹⁷O – H₂O) and 40 mM electrons. Please note the ¹⁷O background due to natural abundance H₂O (for urea and phenol samples) or hardware (i.e., sapphire-rotor and/or stator materials) can be neglected in comparison to the signals arising from the isotopically enriched analytes for this study, although care should be considered when dealing with alternative materials (e.g., Macor, Al₂O₃, ZrO₂), during MAS at higher magnetic fields and / or low ¹⁷O enrichments.

3.2. Dynamic nuclear polarization nuclear magnetic resonance

Dynamic nuclear polarization NMR experiments were performed using a home-built spectrometer equipped with a 5 T (¹H, 212 MHz) wide bore magnet (courtesy of Dr. D. J. Ruben, FBML, MIT) and a 140 GHz gyrotron with 15 W of microwave output. ¹⁷O spectra were recorded using a home-built cryogenic double resonance (¹H and ¹⁷O) DNP NMR probe equipped with a 4 mm Kel-F stator (*Revolution NMR, Fort Collins, CO*). Microwaves were guided to the DNP probe via a circular corrugated, overmoded waveguide to reduce mode conversion and ohmic losses.¹⁰⁷ At the probe entrance, the waveguide tapers to a fundamental mode, from which microwaves are launched towards the sample.^{108, 109} Experimental temperatures for all data were maintained below 88 K. Direct ¹⁷O polarization experiments were acquired with continuous microwave irradiation, while applying a Hahn-echo sequence on ¹⁷O ($\omega_1/2\pi = 180$ kHz, solid (85 K)) using CW or TPPM⁴ proton decoupling ($\omega_1/2\pi > 71$ kHz). Recycle delays were determined via a saturation recovery sequence which accomplishes saturation using the phase cycling scheme described by Daviso et al.¹¹⁰ Polarization buildup (T_B) and spin-lattice relaxation (T_{1I}) times between 4.0 and 6.0 seconds were measured; recycle delays were chosen as $T_B/T_{1I} \times 1.3$.¹¹¹ Directly polarized ¹⁷O detected DNP field-profiles were performed by sweeping the main NMR field using a superconducting sweep coil (± 0.1 T) between 4.961 and 4.996 T (211.7 and 212.3 MHz, ¹H nuclear Larmor frequency). All spectra were referenced with neat water (15 % - H₂ ¹⁷O) to 0 ppm at 298 K. Simulations of ¹⁷O NMR central transition line shapes were performed using SPINEVOLUTION¹¹² and WSOLIDS¹¹³. The SPINEVOLUTION software package was used to fit the ¹⁷O central-transition lineshape by adjusting the C_Q , η and δ_{iso} . Input files are available within the software package and were adjusted to incorporate the experimental conditions used during acquisition, and varying the apodization. WSOLIDS was also used to simulate the ¹⁷O central transition lineshape for the non-spinning data to assist in evaluating the experimental uncertainty. Quadrupolar parameters from GIPAW calculations were simulated without further modification within WSOLIDS. To confirm even excitation for these rather broad ¹⁷O spectra (i.e., ~100 kHz), on-signals were further investigated using a solid (quadrupolar) echo¹¹⁴ as well as

employing the frequency-stepped¹¹⁵ or variable offset cumulative spectra (VOCS)¹¹⁶ method.

3.3. Quantum Chemical Calculations

Electric field gradient and chemical shielding calculations for crystalline ice¹¹⁷, urea¹¹⁸ and phenol¹¹⁹ were performed using a gauge-including projector-augmented wave (GIPAW) density functional theoretical method implemented within CASTEP¹²⁰. The Perdew-Burke-Ernzerhof (PBE) functionals are used in the generalized gradient approximation (GGA) for the exchange-correlation energy^{121, 122} and ultrasoft pseudopotentials.¹²³ All calculations were performed using the fine accuracy basis set and a maximum plane-wave energy of 550 eV in order to calculate both chemical shieldings and electric field gradients.^{124, 125} The Monkhorst-Pack grid had a maximum density of up to $4 \times 4 \times 4$ k points. All calculated chemical shieldings (σ_{cal}) were referenced with respect to (σ_{ref}) 255.0 ppm (Table S1–S3) using ¹H optimized (within CASTEP) crystal structures.¹²⁶

4. Results and Discussion

4.1. Polarizing Agents

Three polarizing agents were studied for direct detection of ¹⁷O, incorporated in a water/glycerol glass-forming cryoprotectant. These water soluble radicals (Figure 1) include TOTAPOL⁵¹, SA-BDPA¹²⁷ and the OX063 version of trityl.¹²⁸

The EPR spectrum of the biradical TOTAPOL introduced by Song et al.⁵¹, largely resembles that of the monomeric TEMPO radical precursor and displays a large *g*-anisotropy resulting in an asymmetric inhomogeneous spectrum with Δ 600 MHz at 5 T. SA-BDPA and trityl are both monomeric radicals and exhibit narrow, approximately symmetric EPR spectra with inhomogeneous linewidths on the order of 28 and 50 MHz, respectively.¹²⁷ We have shown that cross-effect DNP of ¹H followed by cross polarization is the optimal approach thus far in studying a variety of biological systems.^{9, 59, 63, 64, 66, 67, 78, 94, 129, 130}

With the advent of higher powered microwave devices and the use of paramagnetic metal centers, the solid-effect is also of interest, providing significant enhancements can be obtained at elevated fields.¹³¹ To better understand these radicals and the dominant DNP mechanism for direct ¹⁷O polarization we studied ¹⁷O detected field profiles and enhancements.

4.2. Field profiles

Since direct polarization of ¹⁷O is in its naissant we must carefully study both the radical and field profile in order to determine the dominant DNP mechanism for this low- γ nucleus with a nuclear Larmor frequency approximately 1/7th that of ¹H (~28.8 MHz at 5.0 T). Field profiles for each polarizing agent are shown in Figure 2. The DNP field profile obtained using TOTAPOL closely resembles the profile when ¹H's are polarized under similar conditions, exhibiting a slight upfield shift of the DNP maximum (4.9789 T).⁵¹ It is important to note that the maximum negative enhancement (4.9691 T) using the biradical TOTAPOL is actually ~20 % higher than the maximum positive enhancement. The negative lobe of the field profile is also narrower (i.e., sharper) for ¹⁷O than when studying the indirect field profile (i.e., ¹H).⁷⁸ Similar, effects have been seen for directly detected DNP of low- γ nuclei and the polarizing agent TOTAPOL^{77, 85} and bTbk⁸², as a more favorable enhancement is found at the field of maximum negative enhancement. We would like to point out that significant quadrupolar interaction leads to enhanced nuclear relaxation and a broad NMR spectrum that may affect the CE performance. Furthermore, the experiments in

this study are performed on static samples since quadrupolar effects are too strong to be efficiently averaged by magic angle spinning, MAS (see Supp. Info. Figs. S5 and S6) whereas above mentioned experiments on low- γ nuclei have been carried out under MAS conditions.

In contrast to TOTAPOL, SA-BDPA has a narrow ^{17}O field-profile with nearly symmetric positive and negative maxima at 4.9833 and 4.9806 T, respectively. The decreased breadth of the profile is directly related to the significantly narrower EPR spectrum of SA-BDPA with respect to TOTAPOL. This narrow width occurs due to a small inhomogeneity caused by hyperfine coupling to intramolecular ^1H , while the g -tensor anisotropy is vanishing.¹²⁷ Furthermore the isolated positive and negative enhancement peaks are separated by 68 ± 7 MHz in the EPR domain with a flat plateau in the center, indicative of a dominant solid-effect polarization mechanism. However, we note that this separation is significantly larger than the expected separation by $2\omega_{0I} = 57.4$ MHz. The reason for that discrepancy is unclear. It might be caused in part or whole by the relatively low signal enhancement and therefore large error in the extrema of the field profile. At the same time the quadrupolar properties might lead to a slightly different SE matching condition, *vide infra*. In any case, the large separation clearly rules out CE as the DNP mechanism. Trityl exhibits a similar narrow field profile, with symmetric positive (4.9820 T) and negative (4.9808 T) enhancement lobes. The trityl field profile is similar to those of other low- γ nuclei studied (^2H and ^{13}C).^{77, 86} The large ratio of the inhomogeneous breadth, $\Delta \approx 50$ MHz, of the near symmetric EPR spectrum of trityl and the nuclear Larmor frequency, $\omega_{0I} = 29$ MHz (at 5 T), leads to a highly symmetric and unstructured field profile dominated by the CE (see Eq. 2). This is in contrast to other studies of ^{13}C DNP using trityl, where $\Delta \approx \omega_{0I}$ and SE played an equally important role as DNP mechanism besides CE.⁸⁶

The field position of the negative enhancement from trityl and/or SA-BDPA is useful because a slight adjustment in field from the maximum of TOTAPOL for ^1H (4.9798 T) enables one to reach the position for maximum negative DNP enhancement of low- γ nuclei (e.g., ^2H , ^{13}C and ^{17}O) at 4.9808 T. This permits the direct polarization of ^{17}O or other low- γ nuclei using trityl and their indirect polarization via ^1H using TOTAPOL without further adjustment of the external magnetic field.

4.3. Enhancements

To evaluate the efficiency of polarization transfer and enhancements, a series of samples were studied, each using a concentration of 40 mM electron spins of the three polarizing agents. Saturation recovery experiments were performed to determine the effective T_B for direct oxygen detection using SA-BDPA, TOTAPOL, and trityl. Common issues surrounding direct detection for many spins other than ^1H are the long buildup and relaxation times, and the drastic increases in these parameters associated with a decrease in temperature. The combination of the presence of the paramagnetic species in solution, the system being in a disordered state, and oxygen bearing quadrupolar properties (i.e., quadrupolar relaxation) promotes efficient longitudinal relaxation. This enables the use of reasonable recycle delays, comparable to those applied for ^1H . DNP buildup times were measured for each sample; T_B of 5.2, 4.2 and 5.0 seconds were determined for SA-BDPA, TOTAPOL, and trityl, respectively (Table 1).

By maintaining identical sample conditions for SA-BDPA, TOTAPOL, and trityl samples and adjusting only the polarizing agent, the absolute enhancements were determined to be $\epsilon = 3, 7$ and 115, respectively (Table 1, Figure 3). The gain in sensitivity is further increased due to the larger Boltzmann factor at $T = 85$ K, adding gains of approximately 3.5 ($\epsilon^\dagger = 10, 25$ and 400, respectively).

The $I = 5/2$ ^{17}O nucleus poses several differences compared to the typically $I = 1/2$ system (e.g., ^1H , ^{13}C , ^{29}Si , ^{31}P etc.) such as six energy levels (i.e., $\pm 1/2$, $\pm 3/2$ and $\pm 5/2$) and multiple allowed transitions. Furthermore, quadrupolar nuclei in the solid-state experience a significant dispersion of resonance frequencies unless they are situated in a cubic (isotropic) environment. For covalently bound ^{17}O , this dispersion covers a range of up to 9 MHz independent of the external magnetic field strength. Therefore, the matching conditions for the CE and SE in principle are altered to represent the effective Larmor frequency rather than just the Zeeman frequency. This translates the dispersion in the nuclear frequency domain into a dispersion in the matching condition between nuclear spin frequencies and the required irradiation frequency of electron spins, as well as the shape of the DNP field profiles. However, the central transition ($m_I = -1/2 \rightarrow +1/2$) is an exception to this dispersion. The residual second-order broadening of ~ 90 kHz (for ^{17}O in a frozen glass environment at 5 T) can be neglected with respect to the magnitude of the EPR line widths of at least several tens of MHz, and naively, one tends to simply utilize the matching conditions Eqs. (1) and (3).

Nevertheless, several reasons argue against this simplification. The eigenframes of all nuclear m_I states are significantly tilted with respect to the external magnetic field axis absent the fortuitous case of co-linearity between the EFG tensor and the external magnetic field (i.e., the external magnetic field vector is oriented along one of the canonical orientation of the EFG). This tilting leads to significant mixing of the nuclear states. The states are coupled by the non-secular quadrupole interaction components, which are on the order of a few MHz. These couplings are typically much larger than those leading to the electron-nuclear double- and zero-quantum coherences invoked during SE DNP and will therefore affect the state mixing which is a prerequisite for SE. Additional coherences are introduced, which couple the central transition states (i.e., $|m_I| = 1/2$) to those with $|m_I| > 1/2$. Although these transitions are generally off-resonant under SE matching, fast oscillations to these states might compete with the SE transfer and allow for additional nuclear relaxation pathways (vide infra). For the CE, the situation is slightly more complicated because two types of coherences are involved: electron-electron and electron-nuclear dipole coupling between one of the electron spins and the nuclear spin polarized. The former typically is larger than the quadrupole interaction if biradicals are used as polarizing agents (e.g., ~ 25 MHz for TOTAPOL); whereas it approaches the coupling if intermolecular couplings are involved in the case of monoradicals. The electron-nuclear dipole coupling again is expected to be smaller than the nuclear quadrupolar interaction, however, it might also be of similar order since the polarization pathway is less clear than in the SE case. Furthermore, the direct impact of electron-electron and electron-nuclear coupling is not completely understood for the CE, therefore, effects that quadrupolar nuclei impose on the CE efficiency are not clear.

Besides the effect of the quadrupole coupling, non-coherent relaxation processes will affect the DNP transfer. The nuclear quadrupolar interaction leads to very efficient spin-lattice relaxation; competing directly with build-up of enhanced polarization by DNP. Corzilius *et al.*¹³³ have introduced a DNP equilibrium constant K_{DNP} which is calculated from the enhancement factor and takes into account the DNP rate constant k_{DNP} , and the nuclear spin-lattice relaxation time constant T_{1I} :

$$K_{\text{DNP}} = k_{\text{DNP}} T_{1I} = \frac{(\varepsilon_{\infty} - 1)}{\left(\frac{P_S^{\infty}}{P_{I,\text{eq}}} - \varepsilon_{\infty}\right)} \approx \frac{(\varepsilon_{\infty} - 1)}{(\varepsilon_{\text{max}} - \varepsilon_{\infty})} \approx \frac{\varepsilon_{\infty}}{\varepsilon_{\text{max}}} \text{ for } 1 - \varepsilon_{\infty} - \varepsilon_{\text{max}} \quad (9)$$

P_S^{∞} and $P_{I,\text{eq}}$ describe the residual electron polarization after infinite polarization time and the nuclear polarization in thermal equilibrium, respectively; ε_{max} is the thermodynamically maximum achievable enhancement: $\varepsilon_{\text{max}} = \gamma_S/\gamma_I$; and ε_{∞} is the enhancement (ε) after

infinite polarization time. For the first approximation in Eq. (9) it is assumed that the effective electron polarization is not depleted during DNP transfer, which is the case when electron longitudinal relaxation is fast. With this equation we can estimate the effect of fast quadrupolar relaxation on the experimentally observed enhancement. Under this assumption, we find that $K_{\text{DNP}} \ll 1$, so that ε_{max} must be much larger than ε_{∞} . Therefore, we can finally replace $\varepsilon_{\text{max}} - \varepsilon_{\infty}$ with ε_{max} , and $\varepsilon_{\infty} - 1$ with ε_{∞} . In this case, the observed enhancement scales linearly with T_{1I} . We note that T_{1I} only accounts for spin-lattice relaxation including paramagnetic relaxation enhancement (PRE); DNP effects that shorten the experimentally observed time constant have to be excluded. For the SE this is trivial, since DNP is only active when the electron-nuclear spin system is irradiated with the appropriate microwave frequency. In this case, the DNP buildup rate constant and the spin-lattice relaxation rate constant additively form the observed overall buildup rate constant $1/T_B$:

$$\frac{1}{T_B} = k_{\text{DNP}} + \frac{1}{T_{1I}} \quad (10)$$

The CE, however, is always active, because the driving coherences are introduced by the electron-electron coupling, which cannot be switched off; DNP is always active, however, in thermal equilibrium no net polarization transfer occurs because the rates for positive and negative enhancement of nuclear polarization are equal. In this case, net polarization transfer is achieved by disturbing the thermal equilibrium polarization of one of the electron spins by microwave irradiation induced saturation and the resulting change in one of the DNP rate constants. Therefore, a disentanglement of rate constants according to Eq. (10) is not possible.

The observed buildup time constants in Table 1 clearly show a rather uniform distribution with an average of 5.0 s and a small maximum deviation of only 0.8 s. This deviation lies well within the error of the experiments, especially given the small absolute signals when small enhancements are encountered. This leads us to the conclusion that all T_B 's are limited by short T_{1I} , and that k_{DNP} is rather small in all cases. Despite this theoretically unfavorable situation, trityl allows for a significant enhancement of 115, which results in more than a factor of 13,000 reduction of acquisition time. TOTAPOL, on the other hand yields only $\varepsilon = 7$. The discrepancy between trityl and TOTAPOL is explained by the dramatically different EPR lineshapes. While trityl has a Gaussian-like lineshape with $\Delta = 50$ MHz, the overall breadth of the TOTAPOL powder lineshape due to the g-anisotropy is ~ 600 MHz at 5 T. Therefore, the trityl spectrum concentrates the electrons in a more narrow spectral region for efficient ^{17}O CE matching with ω_0 $^{17}\text{O} \sim 29$ MHz. This demonstrates the potential of radicals with a narrow EPR line as effective polarizing agents for CE DNP of low- γ nuclei. We reported similar observations when directly polarizing ^2H .⁷⁷

SA-BDPA yields a rather small enhancement $\varepsilon=3$. We attribute this to the fact that the SE is active in this case, and also be affected by a large quadrupole coupling. Even though a reduction of T_B with respect to T_{1I} is expected for the SE we have observed $T_B \approx T_{1I}$ within the experimental error for all samples, including SA-BDPA. According to Eq. (10) this leads us to conclude that $k_{\text{DNP}} = 1/T_{1I}$ and is in line with the very small observed enhancement. Another potential problem is the depletion of the electron spin polarization by off-resonant saturation of the EPR resonance. The combination of extremely long $T_{1S} = 29$ ms and small resonance offset of $\omega_{0I} = 29$ MHz is supposed to significantly reduce the electron spin polarization available for transfer to nuclear spins by off-resonance irradiation of the EPR transition.¹³¹

It would seem that nuclear relaxation is a significant factor in obtaining effective DNP gains as both ^2H ($\omega_{0I} = 32.5$ MHz, $I=1$) and ^{17}O ($\omega_{0I} = 28.7$ MHz, $I=5/2$) are quadrupolar and

their respective nuclear Larmor frequencies are similar.² H detection on identical samples exhibited an enhancement >500 with a T_B of 70 s, whereas ^{17}O direct detection was $\epsilon=115$ and T_B of 5 s. If ^{17}O $T_{1\rho}$ relaxation rates could be reduced, we surmise that the enhancements would increase.

Further enhancements could be gained from magic-angle spinning at a moderate frequency (figure S6). Rotating the sample has several effects that lead to improved DNP efficiency: including a reduction of certain anisotropies and an increase in the efficiency of polarizing by allowing the microwaves to average over the full surface of the rotor. Our group and others have noted gains in enhancement when studying system under MAS conditions.⁵⁹ We will report on non-spinning and MAS experiments at higher fields in a future publication.

4.4. Mixture

In theory, the CE mechanism is most efficient when two narrow EPR lines are separated by the nuclear Larmor frequency while an appropriate coupling allows for transfer of polarization between the two lines.^{95, 96} The concept has first been demonstrated by Hu *et al.* by mixing the narrow-line radical trityl with the nitroxide radical TEMPO.⁹¹ Irradiation on resonance with the center of the trityl EPR transition resulted in a four-fold increase of enhancement compared to the use of TEMPO as a polarizing agent alone. Therefore a mixture of SA-BDPA and trityl OX063 might allow for cross effect, where the SA-BDPA resonance is irradiated with microwaves and polarization is transferred to a dipolar coupled nucleus during an electron-electron cross-relaxation flip-flop between SA-BDPA and trityl, this approach was illustrated to work extremely well in the case of direct ^{13}C DNP NMR.⁸⁶ In an attempt to improve the enhancement of SA-BDPA, a mixture of 20 mM SA-BDPA and 20 mM trityl in a water/glycerol glass was acquired. The field profile is shown in Figure 2b; the profile indicates a cross-effect mechanism with a broadened inhomogeneous linewidth and a positive maximum (4.982 T). The overall enhancement improved to 40 from 3 (Figure 3). Note that the maximum positive enhancement position coincides with the EPR resonance field of SA-BDPA together with the asymmetry between the positive and negative maxima indicates that the CE is active between SA-BDPA and trityl. The asymmetry was reported by Hu *et al.*⁹¹ and is caused in part by different longitudinal relaxation properties of the radicals involved. In particular, SA-BDPA has a T_{1S} that is significantly longer than that of trityl.¹²⁷ Subsequently, irradiation at the EPR resonance of SA-BDPA leads to a very effective spin saturation, and polarization can be efficiently replenished by fast-relaxing trityl in a cross-relaxation process. Irradiation of the trityl spin on the other hand, would be less efficient due to faster $T_{1\rho}$ relaxation, while cross-relaxation would saturate the slowly relaxing SA-BDPA, effectively quenching the CE.

4.5. Structurally relevant oxygen environments

The ability to polarize ^{17}O directly and indirectly (through ^1H) has enabled this challenging nucleus to be used within a variety of 1D and 2D experiments as a probe for local oxygen environments, which vary within organics, proteins, sugars, surfaces, and oxides. Three common functional groups providing a unique oxygen environment can be envisioned for aiding in structural elucidation of various chemical systems. First, water (H_2O) plays an important role in hydrogen bonding, transport and surface chemistry. Second, carbonyl ($\text{C}=\text{O}$), a double-bonded oxygen, is integral to protein structure, folding and function. Third, hydroxyl ($-\text{OH}$) moiety is often associated with hydration-dehydration reactions, hydrogen bonding, and layered hydroxides. To illustrate the widespread ability of DNP on oxygen environments, ^{17}O spectra of three small molecules are discussed below using direct polarization ^{17}O DNP NMR, room temperature NMR experiments on the crystalline solid (without DNP), and quantum chemical calculations for crystalline water, urea and phenol using GIPAW.

DNP of water environments was recently illustrated using the indirect polarization method via DNP of ^1H followed by cross-polarization.⁷⁸ As water is frozen a variety of arrangements can occur (e.g., Ice-Ih, Ice-XI, etc.) depending on temperature, isotopic content ($^1\text{H} : ^2\text{H}$), freezing rate and pressure.¹³⁴ The frozen solution studied is comprised of a cryoprotecting solvent in an amorphous state, whereby crystal packing is inhibited. Nevertheless, with the significant gains offered by DNP, the quadrupolar NMR parameters can still be determined. A moderate quadrupole coupling constant of 6.8 MHz in magnitude was obtained by spectral simulation of the central transition. The asymmetry parameter and isotropic chemical shift were 0.95 and 0 ppm, respectively, agree well with literature studies of frozen water.^{135, 136} An ordered ice crystal structure¹¹⁷, which apparently occurs at cryogenic temperatures, was calculated using GIPAW in order to evaluate the calculated oxygen NMR properties, crystal structure, and DNP NMR experimental data. The two crystallographic oxygen sites contained quadrupolar coupling constants of -6.632 and -7.034 MHz with asymmetry parameters of 0.91 and 0.88. The averages of these two sites agree well with the experimentally determined parameters above (Figure 4 and Table 2).

Practically all high-field DNP based studies on biological proteins involve a cryoprotecting matrix with approximately 40 % water. This potentially creates a challenge when studying oxygen environments within solutes that need to be dispersed within water as the labeled oxygen sites may compete with the high molarity of the natural abundance oxygen in water (i.e., 55 M oxygen). To illustrate both the major boost in sensitivity of DNP on oxygen and to provide evidence that natural abundant background oxygen is not an issue, organic based carbonyl and hydroxyl small molecules were studied using 3–4 mgs of 30 % labeled ^{17}O . The small sample volume and low enrichments are important aspects for validating DNP as ^{17}O labeling is at present costly and limited concentration within biological solids.¹³⁷

The central transition ^{17}O DNP NMR spectrum of urea, $(\text{NH}_2)_2\text{C}=\text{O}$, a representative $\text{C}=\text{O}$ is shown in Figure 5 with and without microwave radiation. Determining the exact ^{17}O DNP enhancement is difficult due to the poor S/N ratio from the collected off spectrum, nonetheless the enhancement is 80. The quadrupolar coupling parameters ($C_Q = 7.5$ MHz and $\eta = 0.5$) and isotropic chemical shift ($\delta_{\text{iso}} = 150$ ppm) were obtained by spectral simulation (fig. 5b) of the ^{17}O central transition (fig. 5c). The off spectrum was acquired for six days (144 hours) under identical conditions with little success, thus limiting our ability to quantify ϵ . Thus, without DNP this experiment would have been impossible due to the small gyromagnetic ratio, sample volume, and large quadrupolar coupling.

The quadrupolar coupling determined experimentally by DNP and calculated using GIPAW agree quite well with the experimental (non-DNP) solid-state NMR data acquired on crystalline urea¹⁰⁶ (Table 2). One parameter, however, is poorly represented, which is the asymmetry parameter of the cryoprotected small molecule (Figure 5). We experimentally observed $\eta \sim 0.5$, while in the crystalline sample, $\eta \sim 1$ due to the C_{2v} point group symmetry of urea which is the same as for water. Previous studies of crystalline urea by Dong et al.¹⁰⁶ illustrated the importance of incorporating the long-range structure for accurate Gaussian-based calculations in order to calculate the asymmetry parameter properly. With gas-phase based calculations they illustrated that the asymmetry parameter changes from 0.6 to 0.9 as they constructed the surrounding environment around a single urea molecule, indicating that the hydrogen bonding arrangement is important in determining η . Urea solubilized in the cryoprotectant lacks the local environment of the crystalline phase and hence affects the packing, hydrogen bonding, and the effective EFG. Therefore we attribute this change with the EFG to a “solvent effect” that should be considered when studying small molecules with large chemical shieldings or quadrupolar coupling constants as different asymmetry parameters may be observed.^{138, 139}

Phenol, a hydroxyl containing aromatic ring is often associated with tyrosine-like residues and provided $\epsilon > 100$ as shown in Figure 6. As in the case of urea the off signal (acquired for six days) and the on signal (acquired for ~18 hours) exhibited no interference from the oxygen present in the cryoprotectant (or rotor). The lineshape spans over 4,500 ppm (> 130 kHz) with an associated distribution of sites (disordered, glass like structure) causing further broadening of the central region similar to H_2O). The experimental ^{17}O NMR parameters were determined in a fashion similar to that described above with a quadrupolar coupling constant of 8.3 MHz, asymmetry parameter of 0.88 and isotropic chemical shift of 100 ppm. GIPAW calculations and NMR experiments of the crystalline solid (non-DNP) at higher magnetic fields (Table 2, Figure S4) agree well with experimental parameters as well as other phenolic-like systems studied previously.^{100, 140}

Three distinct oxygen environments (i.e., water, carbonyl and hydroxyl) using trityl as a polarizing agent lead to enhancements > 80 . The ability to fit NMR parameters, in particular quadrupolar couplings, which are in reasonable agreement with experimental data acquired at room temperature illustrates the strength of this method for sensitivity gains. The experimentally determined ^{17}O quadrupolar coupling constants from DNP agree well with those obtained from the room temperature NMR data of the crystalline solids (non-DNP) and are reproduced well by the GIPAW based calculations (Figure S1–S3, Tables S1–S3). Although care is advised when recording spectra of quadrupolar and / or highly polarizable nuclei at low temperatures and in a cryoprotecting solvent as both the asymmetry parameter and chemical shielding parameters (i.e., η , δ_{iso} , Ω and κ) are known to be highly sensitive to local chemical environments. DNP is an ideal tool for studying microcrystalline environments which will have limited solvent and temperature effects, enabling the potential to combine DNP with NMR crystallography methods¹⁴² for studying difficult NMR nuclei in other chemical systems.

5. Conclusion

The direct DNP of ^{17}O has been demonstrated on typical oxygen environments relevant to the study of molecular biology. The array of radicals available is vast, however the three most prominent, currently used polarizing agents illustrate the ability to polarize ^{17}O directly without the need of protons. This enables a method to study oxygen environments that lack presence of 1H for CP. Although all radicals discussed provide gains over conventional room temperature NMR, trityl yields the greatest enhancements, while the system offers experimentally convenient relaxation times at cryogenic temperatures. The gains in sensitivity for this spectroscopically difficult quadrupolar nucleus provide significant savings in acquisition time. This provides new opportunities for studying ^{17}O by NMR, enabling extension to multidimensional studies or studies of small sample sizes with isotropic labeling. As DNP moves towards higher magnetic fields and higher frequency spinning this technique should prove promising in the study of biological, medical and material applications.

Supplementary Material

Refer to Web version on PubMed Central for supplementary material.

Acknowledgments

Research reported in this publication was supported by the National Institute of Biomedical Imaging and Bioengineering of the National Institute of Health under award numbers EB-002804, EB-003151, EB-001960, and EB-002026. The authors would like to thank E. Daviso, T.-C. Ong, C. Wilson, A. Thakkar, J. Bryant, R. Lundgren, C. Turner and D. Ruben for valuable discussions throughout the course of this research, Ms. O. Hayes and Prof. T. Swager for supplying the SA-BDPA radical, and Dr. V. Tersikh (National ultrahigh-field NMR Facility for solids,

NRC, Ottawa, Canada) for his assistance with access to the CASTEP software. VKM is grateful to the Natural Sciences and Engineering Research Council of Canada for a postdoctoral fellowship. BC acknowledges receipt of a research fellowship from the Deutsche Forschungsgemeinschaft (CO 802/1-1).

References

1. Pines A, Gibby MG, Waugh JS. Proton-Enhanced Nuclear Induction Spectroscopy. Method for High-Resolution NMR of Dilute Spins in Solids. *J. Chem. Phys.* 1972; 56(4):1776–1777.
2. Andrew ER, Bradbury A, Eades RG. Nuclear Magnetic Resonance Spectra from a Crystal Rotated at High Speed. *Nature.* 1958; 182:1659–1659.
3. Lowe IJ. Free Induction Decays of Rotating Solids. *Physical Review Letters.* 1959; 2(7):285–287.
4. Bennett AE, Rienstra CM, Auger M, Lakshmi KV, Griffin RG. Heteronuclear Decoupling in Rotating Solids. *J. Chem. Phys.* 1995; 103(16):6951–6958.
5. Comellas G, Lopez JJ, Nieuwkoop AJ, Lemkau LR, Rienstra CM. Straightforward, Effective Calibration of SPINAL-64 Decoupling Results in the Enhancement of Sensitivity and Resolution of Biomolecular Solid-State NMR. *J. Magn. Reson.* 2011; 209:131–135. [PubMed: 21296014]
6. Detken A, Hardy EH, Ernst M, Meier BH. Simple And Efficient Decoupling In Magic-Angle Spinning Solid-State NMR: The Xix Scheme. *Chem. Phys. Lett.* 2002; 356:298–304.
7. Fung BM, Khitrin AK, Ermolaev K. An Improved Broadband Decoupling Sequence for Liquid Crystals and Solids. *J. Magn. Reson.* 2000; 142:97–101. [PubMed: 10617439]
8. Rienstra CM, Tucker-Kellogg L, Jaroniec CP, Hohwy M, Reif B, McMahon MT, Tidor B, Lozano-Perez T, Griffin RG. De novo Determination of Peptide Structure with Solid-State Magic-Angle Spinning NMR Spectroscopy. *Proceedings of the National Academy of Sciences of the United States of America.* 2002; 99(16):10260–10265. [PubMed: 12149447]
9. Bajaj VS, Mak-Jurkauskas ML, Belenky M, Herzfeld J, Griffin RG. Functional and Shunt States of Bacteriorhodopsin Resolved by 250 GHz Dynamic Nuclear Polarization-Enhanced Solid-State NMR. *Proc. Natl. Acad. Sci. U. S. A., Early Ed.* 2009; 106:9244–9249.
10. Cady SD, Schmidt-Rohr K, Wang J, Soto C, DeGrado W, Hong M. Structure of the Amantadine Binding Site of Influenza M2 Proton Channels in Lipid Bilayers. *Nature.* 2010; 463:689–692. [PubMed: 20130653]
11. Castellani F, van Rossum B, Diehl A, Schubert M, Rehbein K, Oschkinat H. Structure of a Protein Determined by Solid-State Magic-Angle-Spinning NMR Spectroscopy. *Nature.* 2002; 420(6911): 98–102. [PubMed: 12422222]
12. Eddy MT, Ong T-C, Clark L, Tejjido O, van der Wel PCA, Garces R, Wagner G, Rostovtseva T, Griffin RG. Lipid Dynamics and Protein-Lipid Interactions in 2D Crystals Formed with the B-Barrel Integral Membrane Protein VDAC1. *Journal of the American Chemical Society.* 2012; 134:6375–6387. [PubMed: 22435461]
13. Fitzpatrick AWP, Debelouchina GT, Bayro MJ, Clare DK, Caporini MA, Bajaj VS, Jaroniec CP, Wang L, Ladizhansky V, Mueller SA, et al. Atomic Structure and Hierarchical Assembly of a Cross- β Amyloid Fibril. *Proc Natl Acad Sci U S A.* 2013; 110:5468–5473. [PubMed: 23513222]
14. Jaroniec CP, MacPhee CE, Bajaj VS, McMahon MT, Dobson CM, Griffin RG. High Resolution Molecular Structure of a Peptide in an Amyloid Fibril Determined by MAS NMR Spectroscopy. *Proc. Nat'l. Acad. Sci.* 2004; 101:711–716. [PubMed: 14715898]
15. Linser R, Dasari M, Hiller M, Higman V, Fink U, Amo J-MLd, Markovic S, Handel L, Kessler B, Schmieder P, et al. Proton-Detected Solid-State NMR Spectroscopy Fibrillar and Membrane Proteins. *Angew. Chem. Int. Ed.* 2011; 50:4508–4512.
16. Petkova AT, Ishii Y, Balbach JJ, Antzutkin ON, Leapman RD, Delaglio F, Tycko R. Structural Model for Alzheimer's beta-Amyloid Fibrils Based on Experimental Constraints from Solid State NMR. *Proc. Nat'l Acad Sci.* 2002; 99:16742–16747. [PubMed: 12481027]
17. Tycko R. Progress Towards a Molecular-Level Structural Understanding of Amyloid Fibrils. *Curr Opin Struc Biol.* 2004; 14(1):96–103.
18. Reif B, Jaroniec CP, Rienstra CM, Hohwy M, Griffin RG. H-1-H-1 MAS Correlation Spectroscopy and Distance Measurements in a Deuterated Peptide. *Journal of Magnetic Resonance.* 2001; 151(2):320–327. [PubMed: 11531354]

19. Zhou DH, Graesser DT, Franks WT, Rienstra CM. Sensitivity and Resolution Proton Solid-State NMR at Intermediate Deuteration Levels: Quantitative Linewidth Characterization and Applications to Correlation Spectroscopy. *Journal of Magnetic Resonance*. 2006; 178(2):297–307. [PubMed: 16289756]
20. Lewandowski JR, Dumez J-N, Akbey U, Lange S, Emsley L, Oschkinat H. Enhanced Resolution and Coherence Lifetimes in the Solid-State NMR Spectroscopy Perdeuterated Proteins under Ultrafast Magic Angle Spinning. *Jour. Phys. Chem. Letters*. 2011; 2:2205–2211.
21. Reif B. Ultra-high Resolution in MAS Solid-State NMR of Perdeuterated Proteins: Implications for Structure and Dynamics. *Jour Magn Resonance*. 2012; 216:1–12.
22. Harris RK, Becker ED. NMR Nomenclature: Nuclear Spin Properties and Conventions for Chemical Shifts-IUPAC Recommendations. *Journal of Magnetic Resonance*. 2002; 156:323–326.
23. Wu, G. eMagRes. John Wiley & Sons, Ltd; 2007. Oxygen 17 NMR Studies of Organic and Biological Molecules.
24. Degroot HJM, Harbison GS, Herzfeld J, Griffin RG. Nuclear Magnetic Resonance Study of the Schiff-Base in Bacteriorhodopsin - Counterion Effects on the N-15 Shift Anisotropy. *Biochemistry*. 1989; 28(8):3346–3353. [PubMed: 2742840]
25. Harbison G, Herzfeld J, Griffin RG. N-15 Chemical-Shift Tensors in L-Histidine Hydrochloride Monohydrate. *Journal of the American Chemical Society*. 1981; 103(16):4752–4754.
26. Munowitz M, Bachovchin WW, Herzfeld J, Dobson CM, Griffin RG. Acid-Base and Tautomeric Equilibria in the Solid-State - N-15 Nmr-Spectroscopy of Histidine and Imidazole. *Journal of the American Chemical Society*. 1982; 104(5):1192–1196.
27. Mackenzie, KJD.; Smith, ME. *Multinuclear Solid-State NMR of Inorganic Materials*. Vol. Vol. 6. London: Pergamon; 2002. p. 727
28. Wu G. Solid-State 17O NMR Studies of Organic and Biological Molecules. *Progress in Nuclear Magnetic Resonance Spectroscopy*. 2008; 52:118–169.
29. Prasad S, Clark TM, Sharma R, Kwak HT, Grandinetti PJ, Zimmermann HA. Combined O-17 RAPT and MQ-MAS NMR Study of L-Leucine. *Solid State Nuclear Magnetic Resonance*. 2006; 29(1–3):119–124. [PubMed: 16293400]
30. Brinkmann A, Kentgens APM. Proton-Selective 17O-1H Distance Measurements in Fast Magic-Angle-Spinning Solid-State NMR Spectroscopy for the Determination of Hydrogen Bond Lengths. *Journal of the American Chemical Society*. 2006; 128(46)
31. Chemlka B, Mueller K, Pines A, Stebbins J, Wu Y, Zwanziger J. O-17 NMR in Solids by Dynamic-Angle Spinning and Double Rotation. *Nature*. 1989; 339:42–43.
32. Baltisberger JH, Gann SL, Grandinetti PJ, Pines A. Cross-Polarization Dynamic-Angle Spinning Nuclear Magnetic Resonance of Quadrupolar Nuclei. *Mol. Phys*. 1994; 81:1109.
33. Frydman L, Harwood JS. Isotropic Spectra of Half-Integer Quadrupolar Spins from Bidimensional Magic-Angle Spinning NMR. *J. Am. Chem. Soc*. 1995; 117:5367–5368.
34. Gan Z. Satellite Transition Magic Angle Spinning. *J. Am Chem. Soc*. 2000; 122:3242.
35. Wu G, Rovnyak D, Griffin RG. Quantitative Multiple-Quantum Magic-Angle-Spinning NMR Spectroscopy of Quadrupolar Nuclei in Solids. *Journal of the American Chemical Society*. 1996; 118(39):9326–9332.
36. Wu G, Rovnyak D, Huang PC, Griffin RG. High-Resolution Oxygen-17 NMR Spectroscopy of Solids by Multiple-Quantum Magic-Angle-Spinning. *Chem. Phys. Lett*. 1997; 277(1–3):79–83.
37. Brinkmann A, Kentgens APM. Sensitivity Enhancement and Heteronuclear Distance Measurements in Biological 17O Solid-State NMR. *The Journal of Physical Chemistry B*. 2006; 110(32):16089–16101. [PubMed: 16898766]
38. Gullion T, Yamauchi K, Okonogi M, Asakura T. 13C-17O REAPDOR NMR as a Tool for Determining Secondary Structure in Polyamides. *Macromolecules*. 2007; 40(5):1363.
39. Hung I, Uldry A-C, Becker-Baldus J, Webber AL, Wong A, Smith ME, Joyce SA, Yates JR, Pickard CJ, Dupree R, et al. Probing Heteronuclear 15N-17O and 13C-17O Connectivities and Proximities by Solid-State NMR Spectroscopy. *Journal of the American Chemical Society*. 2009; 131(5):1820–1834. [PubMed: 19138069]
40. Sefzik TH, Houseknecht JB, Clark TM, Prasad S, Lowary TL, Gan Z, Grandinetti PJ. Solid-State 17O NMR in Carbohydrates. *Chem. Phys. Lett*. 2007; 434(4–6):312–315.

41. Wong A, Beevers AJ, Kukol A, Dupree R, Smith ME. Solid-State ^{17}O NMR Spectroscopy Of A Phospholemman Transmembrane Domain Protein: Implications For The Limits Of Detecting Dilute ^{17}O Sites In Biomaterials. *Solid State Nuclear Magnetic Resonance*. 2008; 33(4):72. [PubMed: 18502619]
42. Wu G, Dong S, Ida R, Reen N. A Solid-State ^{17}O Nuclear Magnetic Resonance Study Of Nucleic Acid Bases. *J. Am. Chem. Soc.* 2002; 124(8):1768. [PubMed: 11853455]
43. Yamauchi K, Okonogi M, Kurosu H, Tansho M, Shimizu T, Gullion T, Asakura T. High Field ^{17}O Solid-State NMR Study of Alanine Tripeptides. *Journal of Magnetic Resonance*. 2008; 190(2): 327. [PubMed: 18060815]
44. Zhu J, Ye E, Terskikh V, Wu G. Solid-State ^{17}O NMR Spectroscopy of Large Protein-Ligand Complexes. *Angewandte Chemie, International Edition*. 2010; 49(45):8399–8402.
45. O'Dell LA, Ratcliffe CI, Kong X, Wu G. Multinuclear Solid-State Nuclear Magnetic Resonance and Density Functional Theory Characterization of Interaction Tensors in Taurine. *The Journal of Physical Chemistry A*. 2012; 116(3):1008–1014. [PubMed: 22225526]
46. Wong A, Howes AP, Yates JR, Watts A, Anupold T, Past J, Samoson A, Dupree R, Smith ME. Ultra-High Resolution ^{17}O Solid-State NMR Spectroscopy of Biomolecules: A Comprehensive Spectral Analysis of Monosodium L-Glutamate Monohydrate. *Physical Chemistry Chemical Physics*. 2011; 13(26):12213–12224. [PubMed: 21603686]
47. Becerra LR, Gerfen GJ, Temkin RJ, Singel DJ, Griffin RG. Dynamic Nuclear Polarization with a Cyclotron Resonance Maser at 5 T. *Phys. Rev. Lett.* 1993; 71(21):3561–3564. [PubMed: 10055008]
48. Carver TR, Slichter CP. Polarization of Nuclear Spins in Metals. *Physical Review*. 1953; 92:212–213.
49. Gerfen GJ, Becerra LR, Hall DA, Griffin RG, Temkin RJ, Singel DJ. High Frequency (140 GHz) Dynamic Nuclear Polarization: Polarization Transfer to a Solute in Frozen Aqueous Solution. *J. Chem. Phys.* 1995; 102(24):9494–9497.
50. Overhauser AW. Polarization of Nuclei in Metals. *Phys. Rev.* 1953; 92:411–415.
51. Song C, Hu K-N, Joo C-G, Swager TM, Griffin RG. TOTAPOL – A Biradical Polarizing Agent for Dynamic Nuclear Polarization Experiments in Aqueous Media. *J. Am Chem. Soc.* 2006; 128:11385–11390. [PubMed: 16939261]
52. Dane EL, Corzilius B, Rizzato E, Stocker P, Ouari O, Maly T, Smith AA, Griffin RG, Ouari O, Tordo P, et al. Rigid Orthogonal bis-TEMPO Biradicals with Improved Solubility for Dynamic Nuclear Polarization. *J. Organic Chem.* 2012; 77:1789–1797.
53. Kiesewetter M, Corzilius B, Smith AA, Griffin RG, Swager TM. Dynamic Nuclear Polarization with a Water-soluble Rigid Biradical. *J. Am. Chem. Soc.* 2012; 134:4537–4540. [PubMed: 22372769]
54. Matsuki Y, Maly T, Ouari O, Lyubenova S, Herzfeld J, Prisner T, Tordo P, Griffin RG. Dynamic Nuclear Polarization using a Rigid Biradical. *Angewandte Chemie*. 2009; 48:4996–5000. [PubMed: 19492374]
55. Zagdoun A, Casano G, Ouari O, Lapadula G, Rossini AJ, Lelli M, Baffert M, Gajan D, Veyre L, Maas WE, et al. A Slowly Relaxing Rigid Biradical for Efficient Dynamic Nuclear Polarization Surface-Enhanced NMR Spectroscopy: Expedient Characterization of Functional Group Manipulation in Hybrid Materials. *J. Am. Chem. Soc.* 2012; 134:2284–2291. [PubMed: 22191415]
56. Zagdoun A, Casano G, Ouari O, Schwarzwälder M, Rossini AJ, Aussenac F, Yulikov M, Jeschke G, Copéret C, Lesage A, et al. Large Molecular Weight Nitroxide Biradicals Providing Efficient Dynamic Nuclear Polarization at Temperatures up to 200 K. *Journal of the American Chemical Society*. 2013; 135(34):12790–12797. [PubMed: 23961876]
57. Hall DA, Maus DC, Gerfen GJ, Inati SJ, Becerra LR, Dahlquist FW, Griffin RG. Polarized-Enhanced NMR Spectroscopy of Biomolecules in Frozen Solution. *Science*. 1997; 276(5314): 930–932. [PubMed: 9139651]
58. Rosay M, Lansing JC, Haddad KC, Bachovchin WW, Herzfeld J, Temkin RJ, Griffin RG. High-Frequency Dynamic Nuclear Polarization in MAS Spectra of Membrane and Soluble Proteins. *J. Am. Chem. Soc.* 2003; 125(45):13626–13627. [PubMed: 14599177]

59. Rosay M, Tometich L, Pawsey S, Bader R, Schauwecker R, Blank M, Borchard PM, Cauffman SR, Felch KL, Weber RT, et al. Solid-State Dynamic Nuclear Polarization at 263 GHz: Spectrometer Design and Experimental Results. *Phys. Chem. Chem. Phys.* 2010; 12(22):5850–5860. [PubMed: 20449524]
60. Rosay M, Weis V, Kreischer KE, Temkin RJ, Griffin RG. Two-Dimensional ¹³C-¹³C Correlation Spectroscopy with Magic Angle Spinning and Dynamic Nuclear Polarization. *J. Am. Chem. Soc.* 2002; 124(13):3214–3215. [PubMed: 11916398]
61. Rosay M, Zeri AC, Astrof NS, Opella SJ, Herzfeld J, Griffin RG. Sensitivity-Enhanced NMR Of Biological Solids: Dynamic Nuclear Polarization Of Y21M Fd Bacteriophage And Purple Membrane. *Journal of the American Chemical Society.* 2001; 123(5):1010–1011. [PubMed: 11456650]
62. Akbey U, Franks WT, Linden A, Lange S, Griffin RG, van RB-J, Oschkinat H. Dynamic Nuclear Polarization of Deuterated Proteins. *Angew. Chem., Int. Ed.* 2010; 49(42):7803–7806.
63. Bayro MJ, Debelouchina GT, Eddy MT, Birkett NR, MacPhee CE, Rosay M, Maas WE, Dobson CM, Griffin RG. Intermolecular Structure Determination of Amyloid Fibrils with Magic-Angle Spinning and Dynamic Nuclear Polarization NMR. *J. Am. Chem. Soc.* 2011; 133(35):13967–13974. [PubMed: 21774549]
64. Debelouchina GT, Bayro MJ, van dWPCA, Caporini MA, Barnes AB, Rosay M, Maas WE, Griffin RG. Dynamic Nuclear Polarization-Enhanced Solid-State NMR Spectroscopy of GNNQQNY Nanocrystals and Amyloid Fibrils. *Phys. Chem. Chem. Phys.* 2010; 12(22):5911–5919. [PubMed: 20454733]
65. Lelli M, Gajan D, Lesage A, Caporini MA, Vitzthum V, Mieville P, Heroguel F, Rascon F, Roussey A, Thieuleux C, et al. Fast Characterization of Functionalized Silica Materials by Silicon-29 Surface-Enhanced NMR Spectroscopy using Dynamic Nuclear Polarization. *J. Am. Chem. Soc.* 2011; 133(7):2104–2107. [PubMed: 21280606]
66. Mak-Jurkauskas ML, Bajaj VS, Hornstein MK, Belenky M, Griffin RG, Herzfeld J. Energy Transformations Early in the Bacteriorhodopsin Photocycle Revealed by DNP-Enhanced Solid-State NMR. *Proc. Natl. Acad. Sci. U. S. A.* 2008; 105(3):883–888. [PubMed: 18195364]
67. Van der Wel PCA, Hu K-N, Lewandowski J, Griffin RG. Dynamic Nuclear Polarization of Amyloidogenic Peptide Nanocrystals: GNNQQNY, a Core Segment of the Yeast Prion Protein Sup35p. *J. Am. Chem. Soc.* 2006; 128(33):10840–10846. [PubMed: 16910679]
68. Lafon O, Thankamony ASL, Kobayashi T, Carnevale D, Vitzthum V, Slowing II, Kandel K, Vezin H, Amoureux J-P, Bodenhausen G, et al. Mesoporous Silica Nanoparticles Loaded with Surfactant: Low Temperature Magic Angle Spinning ¹³C and ²⁹Si NMR Enhanced by Dynamic Nuclear Polarization. *The Journal of Physical Chemistry C.* 2012; 117(3):1375–1382.
69. Takahashi H, Ayala I, Bardet M, De Paëpe G, Simorre J-P, Hediger S. Solid-State NMR on Bacterial Cells: Selective Cell Wall Signal Enhancement and Resolution Improvement using Dynamic Nuclear Polarization. *Journal of the American Chemical Society.* 2013; 135(13):5105–5110. [PubMed: 23362837]
70. Ravera E, Corzilius B, Michaelis VK, Rosa C, Griffin RG, Luchinat C, Bertini I. Dynamic Nuclear Polarization of Sedimented Solutes. *Journal of the American Chemical Society.* 2013; 135(5):1641–1644. [PubMed: 23331059]
71. Gelis I, Vitzthum V, Dhimole N, Caporini M, Schedlbauer A, Carnevale D, Connell S, Fucini P, Bodenhausen G. Solid-State NMR Enhanced by Dynamic Nuclear Polarization as a Novel Tool for Ribosome Structural Biology. *J Biomol NMR.* 2013; 56(2):85–93. [PubMed: 23689811]
72. Lesage A, Lelli M, Gajan D, Caporini MA, Vitzthum V, Mieville P, Alauzun J, Roussey A, Thieuleux C, Medhi A, et al. Surface Enhanced NMR Spectroscopy by Dynamic Nuclear Polarization. *Journal of the American Chemical Society.* 2010; 132:15459–14461. [PubMed: 20831165]
73. Ong T-C, Mak-Jurkauskas ML, Walsh JJ, Michaelis VK, Corzilius B, Smith AA, Clausen AM, Cheetham JC, Swager TM, Griffin RG. Solvent-Free Dynamic Nuclear Polarization of Amorphous and Crystalline ortho-Terphenyl. *The Journal of Physical Chemistry B.* 2013; 117(10):3040–3046. [PubMed: 23421391]

74. Potapov A, Yau W-M, Tycko R. Dynamic Nuclear Polarization-Enhanced ^{13}C NMR Spectroscopy of Static Biological Solids. *Journal of Magnetic Resonance*. 2013; 231(0):5–14. [PubMed: 23562665]
75. Rossini AJ, Zagdoun A, Hegner F, Schwarzwälder M, Gajan D, Copéret C, Lesage A, Emsley L. Dynamic Nuclear Polarization NMR Spectroscopy of Microcrystalline Solids. *Journal of the American Chemical Society*. 2012; 134(40):16899–16908. [PubMed: 22967206]
76. Takahashi H, Hediger S, De Paepe G. Matrix-Free Dynamic Nuclear Polarization Enables Solid-State NMR ^{13}C - ^{13}C Correlation Spectroscopy of Proteins at Natural Isotopic Abundance. *Chemical Communications*. 2013
77. Maly T, Andreas LB, Smith AA, Griffin RG. ^2H -DNP-Enhanced ^2H - ^{13}C Solid-State NMR Correlation Spectroscopy. *Physical Chemistry Chemical Physics*. 2010; 12(22):5872–5878. [PubMed: 20458422]
78. Michaelis VK, Markhasin E, Daviso E, Herzfeld J, Griffin RG. Dynamic Nuclear Polarization of Oxygen-17. *The Journal of Physical Chemistry Letters*. 2012; 3:2030–2034. [PubMed: 23024834]
79. Vitzthum V, Caporini MA, Bodenhausen G. Solid-State Nitrogen-14 Nuclear Magnetic Resonance Enhanced by Dynamic Nuclear Polarization using a Gyrotron. *Journal of Magnetic Resonance*. 2010; 205:177–179. [PubMed: 20488737]
80. Vitzthum V, Mieville P, Carnevale D, Caporini MA, Gajan D, Coperet C, Lelli M, Zagdoun A, Rossini AJ, Lesage A. Dynamic Nuclear Polarization of Quadrupolar Nuclei using Cross Polarization from Protons: Surface-Enhanced Aluminium-27 NMR. *Chemical Communications*. 2012; 48(14):1988–1990. [PubMed: 22237253]
81. Lee D, Takahashi H, Thankamony ASL, Dacquin JP, Bardet M, Lafon O, De Paepe G. Enhanced Solid-State NMR Correlation Spectroscopy of Quadrupolar Nuclei using Dynamic Nuclear Polarization. *Journal of the American Chemical Society*. 2012; 134(45):18491–18494. [PubMed: 23095121]
82. Blanc F, Sperrin L, Jefferson DA, Pawsey S, Rosay M, Grey CP. Dynamic Nuclear Polarization Enhanced Natural Abundance ^{17}O Spectroscopy. *Journal of the American Chemical Society*. 2013; 135(8):2975–2978. [PubMed: 23379257]
83. Lafon O, Rosay M, Aussenac F, Lu X, Trebosc J, Cristini O, Kinowski C, Touati N, Vezin H, Amoureux J-P. Beyond the Silica Surface by Direct Silicon-29 Dynamic Nuclear Polarization. *Angewandte Chemie*. 2011; 50(36):8367–8370. [PubMed: 21770004]
84. Lafon O, Thankamony ASL, Rosay M, Aussenac F, Lu X, Trebosc J, Bout-Roumazielles V, Vezin H, Amoureux J-P. Indirect and Direct ^{29}Si Dynamic Nuclear Polarization of Dispersed Nanoparticles. *Chemical Communications*. 2013; 49(28):2864–2866. [PubMed: 23238047]
85. Maly T, Miller AF, Griffin RG. In Situ High-Field Dynamic Nuclear Polarization-Direct and Indirect Polarization of ^{13}C Nuclei. *Chemphyschem*. 2010; 11(5):999–1001. [PubMed: 20169604]
86. Michaelis VK, Smith AA, Corzilius B, Haze O, Swager TM, Griffin RG. High-Field ^{13}C Dynamic Nuclear Polarization with a Radical Mixture. *Journal of the American Chemical Society*. 2013; 135(8):2935–2938. [PubMed: 23373472]
87. Wind RA, Duijvestijn MJ, Vanderlugt C, Manenschijn A, Vriend J. Applications of Dynamic Nuclear-Polarization in ^{13}C NMR in Solids. *Progress in Nuclear Magnetic Resonance Spectroscopy*. 1985; 17:33–67.
88. Hu, K-N.; Iuga, D.; Griffin, RG. DNP enhanced ^{17}O SSNMR Spectroscopy on Biological Solids; Experimental NMR Conference; Asilomar, CA. Asilomar, CA: 2003. p. 317
89. Michaelis, VK.; Markhasin, E.; Daviso, E.; Corzilius, B.; Smith, A.; Herzfeld, J.; Griffin, RG. DNP NMR of Oxygen-17 using Mono- and Bi-radical Polarizing Agents; Experimental NMR Conference; Miami, FL. Miami, FL: 2012.
90. Corzilius B, Smith AA, Barnes AB, Luchinat C, Bertini I, Griffin RG. High-Field Dynamic Nuclear Polarization with High-Spin Transition Metal Ions. *Journal of the American Chemical Society*. 2011; 133:5648–5651. [PubMed: 21446700]
91. Hu K, Bajaj V, Rosay M, Griffin R. High-Frequency Dynamic Nuclear Polarization using Mixtures of TEMPO and Trityl Radicals. *J Chem Phys*. 2007; 126(4):044512–044517. [PubMed: 17286492]

92. Hwang CF, Hill DA. Phenomenological Model for New Effect in Dynamic Polarization. *Physical Review Letters*. 1967; 19
93. Kessenikh AV, Lushchikov VI, Manenkov AA, Taran YV. Proton Polarization in Irradiated Polyethylenes. *Sov. Phys. Solid State*. 1963; 5:321–329.
94. Maly T, Debelouchina GT, Bajaj VS, Hu KN, Joo CG, Mak-Jurkauskas ML, Sirigiri JR, van der Wel PCA, Herzfeld J, Temkin RJ, et al. Dynamic Nuclear Polarization at High Magnetic Fields. *J. Chem. Phys.* 2008; 128(5):052211–052219. [PubMed: 18266416]
95. Wollan DS. Dynamic Nuclear-Polarization with an Inhomogeneously Broadened ESR Line 1. Theory. *Physical Review B*. 1976; 13(9):3671–3685.
96. Wollan DS. Dynamic Nuclear-Polarization with an Inhomogeneously Broadened ESR Line 2. Experiment. *Physical Review B*. 1976; 13(9):3686–3696.
97. Abragam, A. *Principles of Nuclear Magnetic Resonance*. New York: Oxford University Press; 1961.
98. Slichter, CP. *Principles of Magnetic Resonance*. New York: Harper & Row; 1963.
99. Taulelle, F. *NMR of Quadrupolar Nuclei in the Solid State*. Vol. 322. London: Kluwer Academic Publishers; 1988. p. 476
100. Lemaitre V, Smith ME, Watts A. A Review of Oxygen-17 Solid-State NMR of Organic Materials - Towards Biological Applications. *Solid State Nucl. Magn. Reson.* 2004; 26(3–4):215–235. [PubMed: 15388187]
101. Pike KJ, Lemaitre V, Kukol A, Anupold T, Samoson A, Howes AP, Watts A, Smith ME, Dupree R. Solid-State ¹⁷O NMR of Amino Acids. *J. Phys. Chem. B*. 2004; 108(26):9256–9263.
102. Wu, G. *Encyclopedia of Magnetic Resonance*. Wiley; 2011. Oxygen 17 NMR Studies of Organic and Biological Molecules.
103. Ashbrook, SE.; Wimperis, S. *eMagRes*. John Wiley & Sons, Ltd; 2007. Quadrupolar Coupling: An Introduction and Crystallographic Aspects.
104. Fernandez C, Pruski M. Probing Quadrupolar Nuclei by Solid-State NMR Spectroscopy: Recent Advances. *Topics In Current Chemistry*. 2012; 306:119–188. [PubMed: 21656101]
105. Man, PP. *Encyclopedia of Analytical Chemistry*. Chichester: John Wiley and Sons; 2000. p. 12224–12265.
106. Dong S, Ida R, Wu G. A Combined Experimental and Theoretical ¹⁷O NMR Study of Crystalline Urea: An Example of Large Hydrogen-Bonding Effects. *The Journal of Physical Chemistry A*. 2000; 104:11194–11202.
107. Woskov PW, Bajaj VS, Hornstein MK, Temkin RJ, Griffin RG. Corrugated Waveguide and Directional Coupler for CW 250 GHz Gyrotron DNP Experiments. *IEEE Transactions on Microwave Theory and Techniques*. 2005; 53:1863–69. [PubMed: 17901907]
108. Becerra LR, Gerfen GJ, Bellew BF, Bryant JA, Hall DA, Inati SJ, Weber RT, Un S, Prisner TF, McDermott AE, et al. A Spectrometer for Dynamic Nuclear-Polarization and Electron-Paramagnetic-Resonance at High-Frequencies. *Journal of Magnetic Resonance Series A*. 1995; 117(1):28–40.
109. Barnes AB, Mak-Jurkauskas ML, Matsuki Y, Bajaj VS, Wel PCAvd, DeRocher R, Bryant J, Sirigiri JR, Temkin RJ, Lugtenburg J, et al. Cryogenic sample exchange NMR probe for magic angle spinning dynamic nuclear polarization. *Jour. Magnetic Resonance*. 2009; 198:261–270.
110. Daviso E, Diller A, Alia A, Matysik J, Jeschke G. Photo-CIDNP MAS NMR Beyond the T(1) Limit by Fast Cycles of Polarization Extinction and Polarization Generation. *Journal of Magnetic Resonance*. 2008; 190(1):43–51. [PubMed: 17967555]
111. Pons M, Feliz M, Giralt E. Steady-State DQF-COSY Spectra Using a Variable Relaxation Delay. *Journal of Magnetic Resonance*. 1988; 78:314–320.
112. Veshkort M, Griffin RG. Spinevolution: A Powerful Tool for the Simulation of the Solid and Liquid State NMR Experiments. *Journal of Magnetic Resonance*. 2006; 178(2):248–282. [PubMed: 16338152]
113. Eichele K. *WSolids NMR Simulation Package*. 2013 1.20.21.

114. Davis JH, Jeffrey KR, Bloom M, Valic MI, Higgs TP. Quadrupolar Echo Deuteron Magnetic Resonance Spectroscopy in Ordered Hydrocarbon Chains. *Chem. Phys. Lett.* 1976; 42(2):390–394.
115. Rhodes HE, Wang PK, Stokes HT, Slichter CP, Sinfelt JH. NMR of Platinum Catalysts. 1 Line Shapes. *Physical Review B.* 1982; 26(7):3559–3568.
116. Massiot D, Farnan I, Gautier N, Trumeau D, Trokiner A, Coutures JP. Ga-71 and Ga-69 Nuclear Magnetic Resonance Study of Beta-Ga₂O₃ Resolution of 4-fold and 6-fold Coordinated Ga Sites in Static Conditions. *Solid State Nuclear Magnetic Resonance.* 1995; 4(4):241–248. [PubMed: 7583059]
117. Bernal JD, Fowler RH. A Theory of Water and Ionic Solution, with Particular Reference to Hydrogen and Hydroxyl Ions. *J. Chem. Phys.* 1933; 1:515–548.
118. Sklar N, Senko ME, Post B. Thermal Effects in Urea - Crystal Structure at -140 degrees C and at Room Temperature. *Acta Crystallographica.* 1961; 14:716–720.
119. Scheringer C. Die Kristallstruktur des Phenols. *Zeitschrift fuer Kristallographie.* 1963; 119:273–283.
120. Clark SJ, Segall MD, Pickard CJ, Hasnip PJ, Probert MJ, Refson K, Payne MC. First Principles Methods using CASTEP. *Zeitschrift fuer Kristallographie.* 2005; 220(5–6):567–570.
121. Perdew JP, Burke K, Ernzerhof M. Generalized Gradient Approximation Made Simple. *Physical Review Letters.* 1996; 77:3865–3868. [PubMed: 10062328]
122. Perdew JP, Burke K, Ernzerhof M. Generalized Gradient Approximation Made Simple -Reply. *Physical Review Letters.* 1998; 80:891–891.
123. Vanderbilt D. Soft Self-Consistent Pseudopotentials In A Generalized Eigenvalue Formalism. *Physical Review B.* 1990; 41(11):7892–7895.
124. Profeta M, Mauri F, Pickard CJ. Accurate First Principles Prediction of ¹⁷O NMR Parameters in SiO₂: Assignment of the Zeolite Ferrierite Spectrum. *Journal of the American Chemical Society.* 2003; 125:541–548. [PubMed: 12517169]
125. Yates JR, Pickard CJ, Mauri F. Calculation of NMR Chemical Shifts for Extended Systems using Ultrasoft Pseudopotentials. *Physical Review B.* 2007; 76:024401–024411.
126. Yates JR, Pickard CJ, Payne MC, Dupree R, Profeta M, Mauri F. Theoretical Investigation of Oxygen-17 NMR Shielding and Electric Field Gradients in Glutamic Acid Polymorphs. *Journal of Physical Chemistry A.* 2004; 108:6032–6037.
127. Haze O, Corzilius B, Smith AA, Griffin RG, Swager TM. Water-Soluble Narrow Line Radicals for Dynamic Nuclear Polarization. *J. Am. Chem. Soc.* 2012; 134:14287–14290. [PubMed: 22917088]
128. Thaning M. Free Radicals. 2000
129. Barnes AB, De Paepe G, van der Wel PCA, Hu KN, Joo CG, Bajaj VS, Mak-Jurkauskas ML, Sirigiri JR, Herzfeld J, Temkin RJ, et al. High-Field Dynamic Nuclear Polarization for Solid and Solution Biological NMR. *Appl. Magn. Reson.* 2008; 34(3–4):237–263. [PubMed: 19194532]
130. Hu K-N, Yu H-H, Swager TM, Griffin RG. Dynamic Nuclear Polarization with Biradicals. *J. Am. Chem. Soc.* 2004; 126(35):10844–10845. [PubMed: 15339160]
131. Smith AA, Corzilius B, Barnes AB, Maly T, Griffin RG. Solid Effect Dynamic Nuclear Polarization and Polarization Pathways. *J. Chem. Phys.* 2012; 136 015101-(1–16).
132. Corzilius B, Andreas LB, Smith AA, Ni QZ, Griffin RG. Paramagnet Induced Signal Quenching in MAS-DNP Experiments on Homogeneous Solutions. *Journal of Magnetic Resonance.* 2013 Submitted.
133. Corzilius B, Smith AA, Griffin RG. Solid Effect in Magic Angle Spinning Dynamic Nuclear Polarization. *J. Chem. Phys.* 2012; 137:054201–054212. [PubMed: 22894339]
134. Salzmann CG, Radaelli PG, Hallbrucker A, Mayer E, Finney JL. The Preparation and Structures of Hydrogen Ordered Phases of Ice. *Science.* 2006; 311(5768):1758–1761. [PubMed: 16556840]
135. Spiess HW, Garrett BB, Sheline RK. Oxygen-17 Quadrupole Coupling Parameters for Water in its Various Phases. *J. Chem. Phys.* 1969; 51(3):1201–1205.

136. Ba Y, Ripmeester JA, Ratcliffe CI. Water Molecular Reorientation in Ice and Tetrahydrofuran Clathrate Hydrate from Lineshape Analysis of ^{17}O Spin-Echo NMR Spectra. *Canadian Journal of Chemistry*. 2011; 89:1055–1064.
137. Antzutkin ON, Iuga D, Filippov AV, Kelly RT, Becker-Baldus J, Brown SP, Dupree R. Hydrogen Bonding in Alzheimer's Amyloid- β Fibrils Probed by $^{15}\text{N}\{^{17}\text{O}\}$ REAPDOR Solid-State NMR Spectroscopy. *Angewandte Chemie International Edition*. 2012; 51(41):10289–10292.
138. Stringfellow TC, Farrar TC. Temperature Dependence of the ^{14}N Quadrupole Coupling Constant of Isocyanomethane. *J. Chem. Phys.* 1995; 102(24):9465–9473.
139. Lucken, EAC. Nuclear Quadrupole Coupling Constants. London: Academic; 1969.
140. Zhu J, Lau JYC, Wu G. A Solid-State ^{17}O NMR Study of L-Tyrosine in Different Ionization States: Implications for Probing Tyrosine Side Chains in Proteins. *Journal of Physical Chemistry B*. 2010; 114:11681–11688.
141. Herzfeld J, Berger AE. Sideband Intensities in NMR-Spectra of Samples Spinning at the Magic Angle. *J. Chem. Phys.* 1980; 73(12):6021–6030.
142. Harris, RK.; Wasylishen, RE.; Duer, MJ. *NMR Crystallography*. 1 ed.. Wiley, John & Sons; 2009.

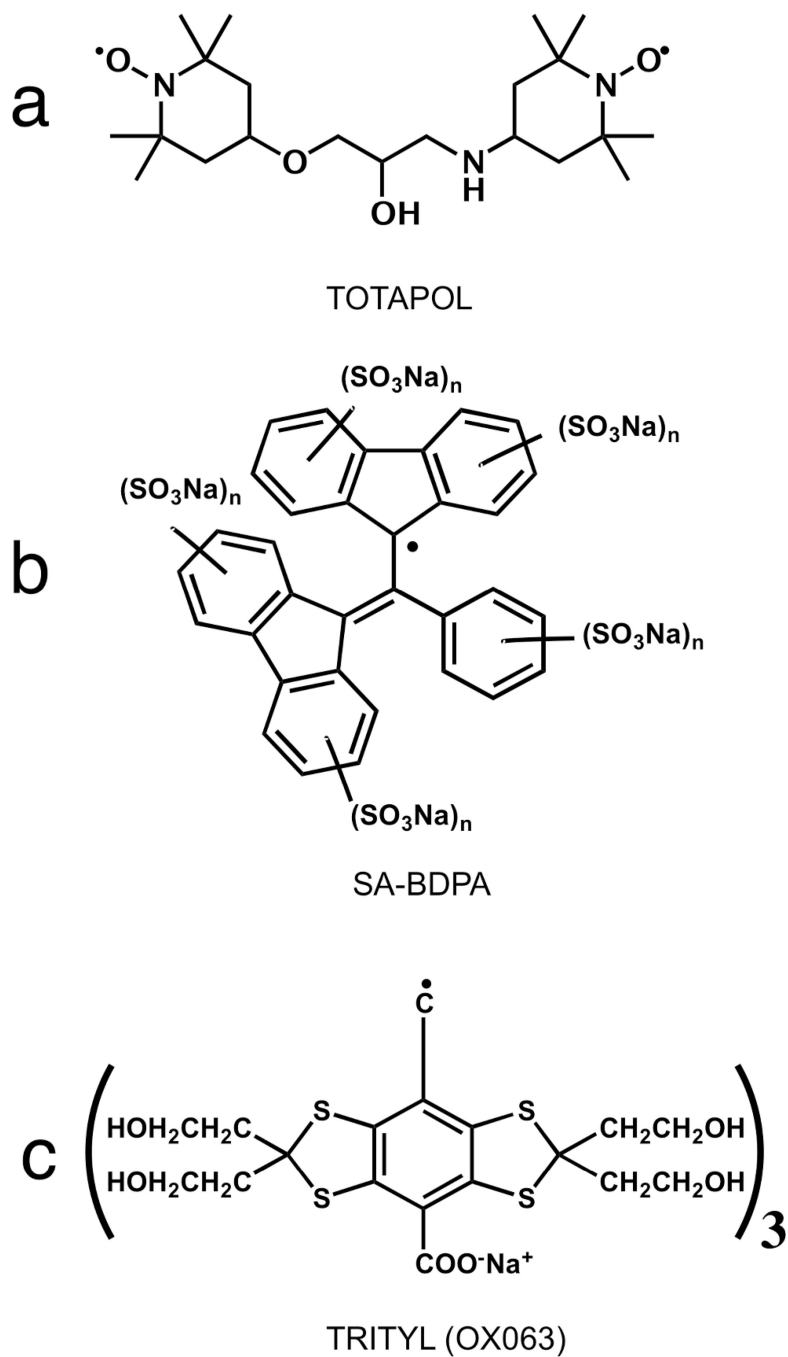


Figure 1. Molecular structures for (a) TOTAPOL (bi-radical), (b) SA-BDPA (mono-radical) and (c) trityl-OX063 (mono-radical) polarizing agents capable of directly polarizing ^{17}O .

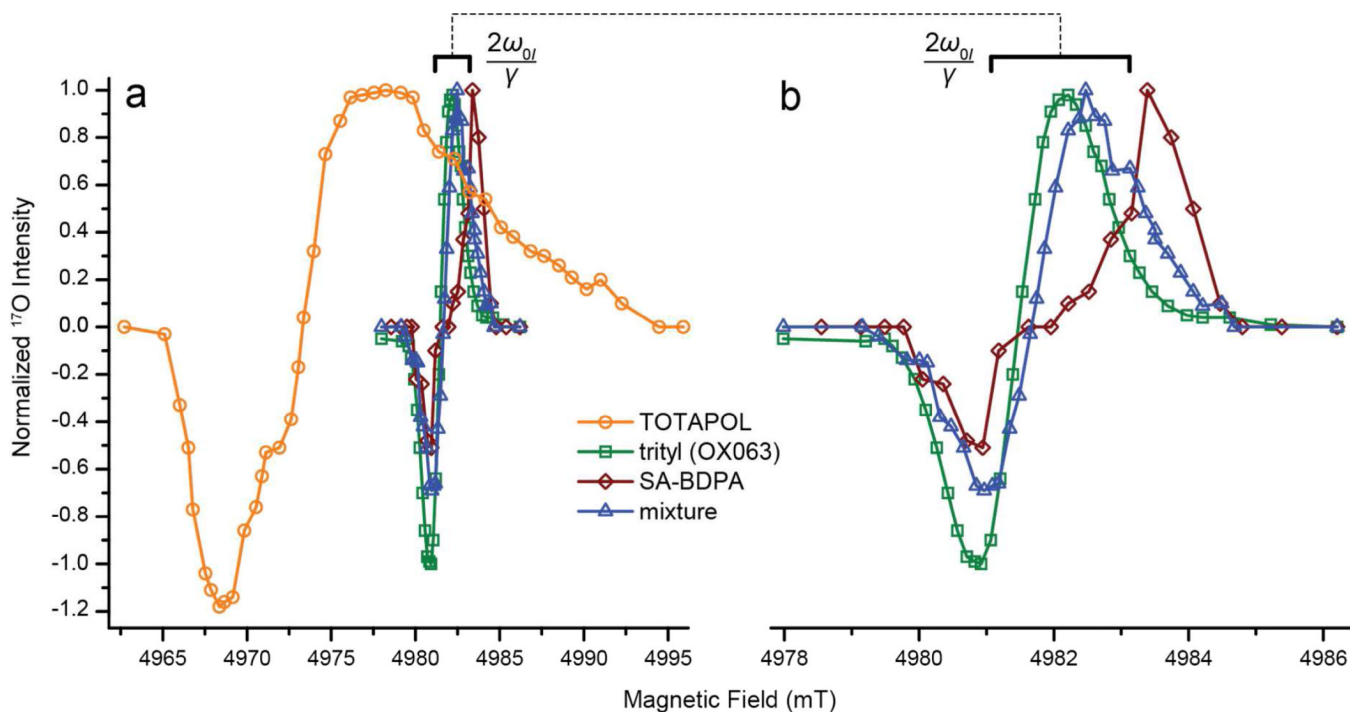


Figure 2.

(a) ^{17}O detected field profiles for (circle, orange) TOTAPOL (96 scans / point), (square, green) trityl (8 scans / point), (diamond, red) SA-BDPA (384 scans / point) and (triangle, blue) SA-BDPA-trityl mixture (16 scans / point). (b) Expanded region for the three narrow-line radical field profiles. Sample composition for field profiles was 60/40 (v/v) d_8 -glycerol/ H_2 ^{17}O (35% - ^{17}O - H_2O) with 40 mM electrons.

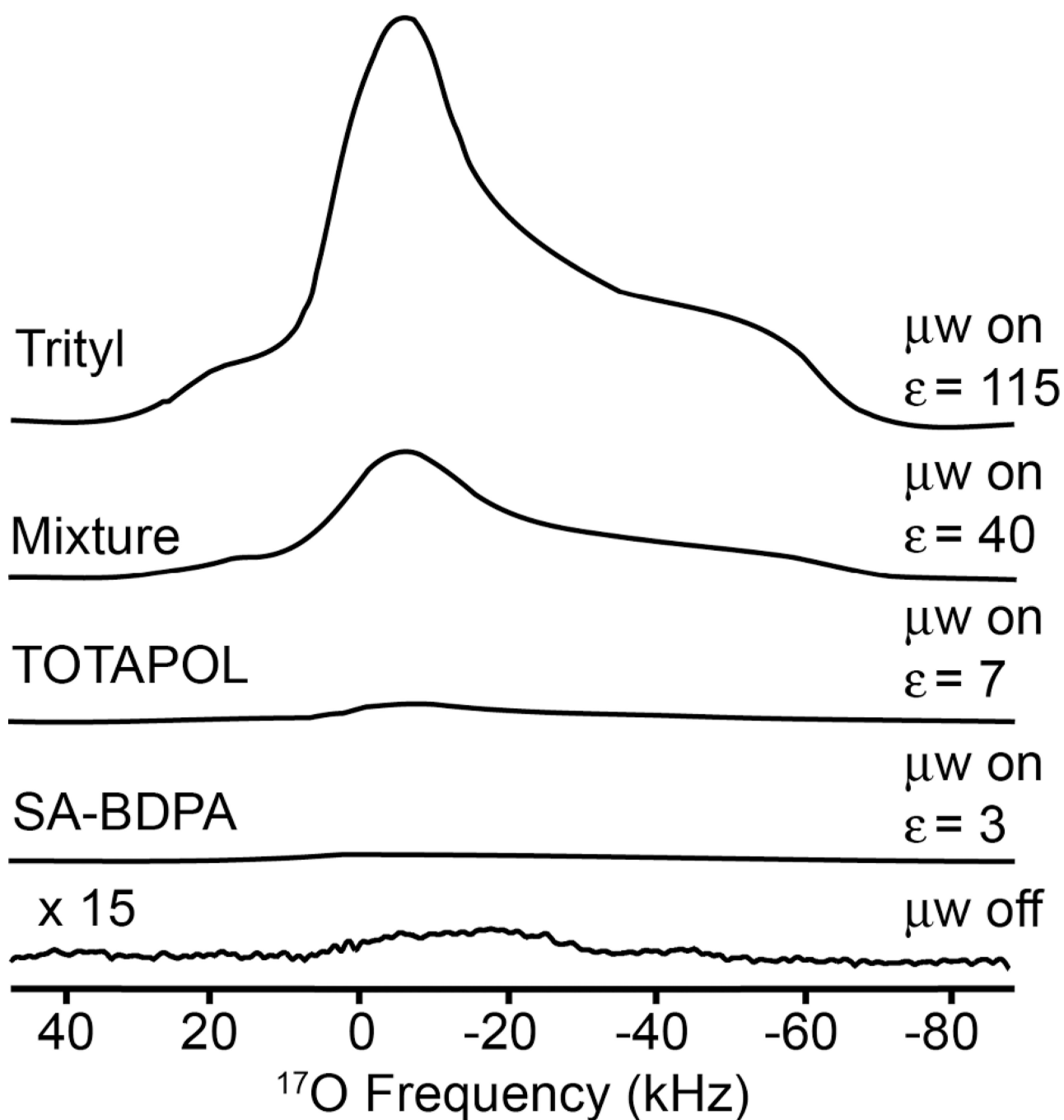


Figure 3.

Direct polarization of ^{17}O in 60/30/10 (v/v) d_8 -glycerol/ $\text{D}_2\text{O}/\text{H}_2$ ^{17}O using 35% labeled ^{17}O water and 40 mM electrons, using 9 W of microwave power. Radicals are arranged from highest enhancement to lowest, with trityl (16 scans, ~2 minutes), mixture (64 scans, ~8 minutes), TOTAPOL (608 scans, ~60 minutes) and SA-BDPA (1,664 scans and ~180 minutes), and, the microwaves off x15 (6,646 scans, ~12 hours) spectrum from the trityl sample. NB: Enhancements and uncertainties in Table 1 were determined by acquiring an on/off signal on the same sample; the bottom trace in the figure is the off spectrum for the trityl radical and is included here for reference purposes.

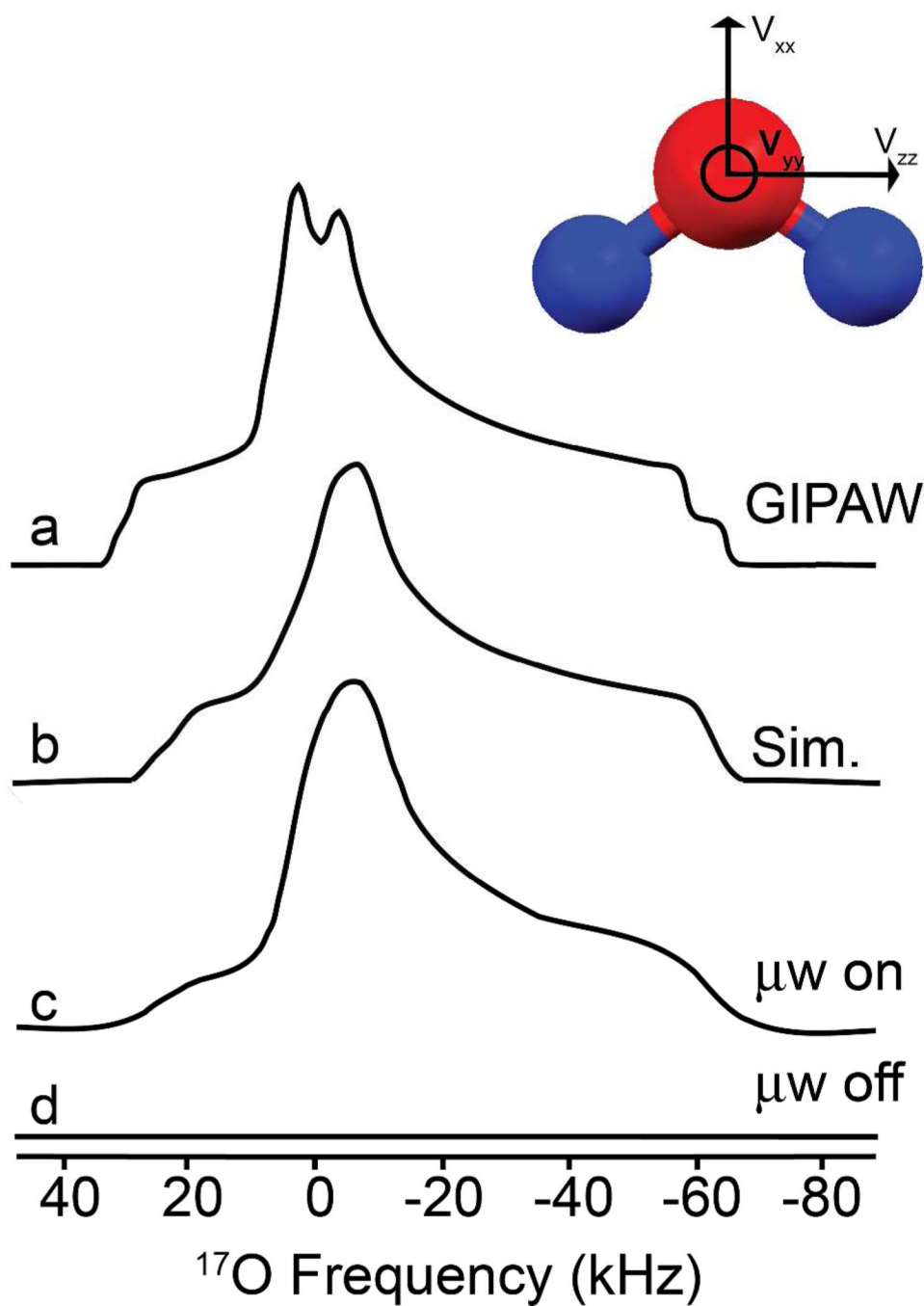


Figure 4. ^{17}O DNP NMR spectrum of water using direct polarization from trityl. a) Simulation using GIPAW calculated parameters for crystal structure, b) simulation of quadrupolar lineshape, c) experiment on-signal for amorphous sample (64 scans, ~7 minutes) and d) experiment off-signal (6646 scans, ~12 hours). Sample conditions: 60/30/10 (v/v) d_8 -glycerol/ D_2O / H_2 ^{17}O using 35% labeled ^{17}O water and 40 mM trityl.

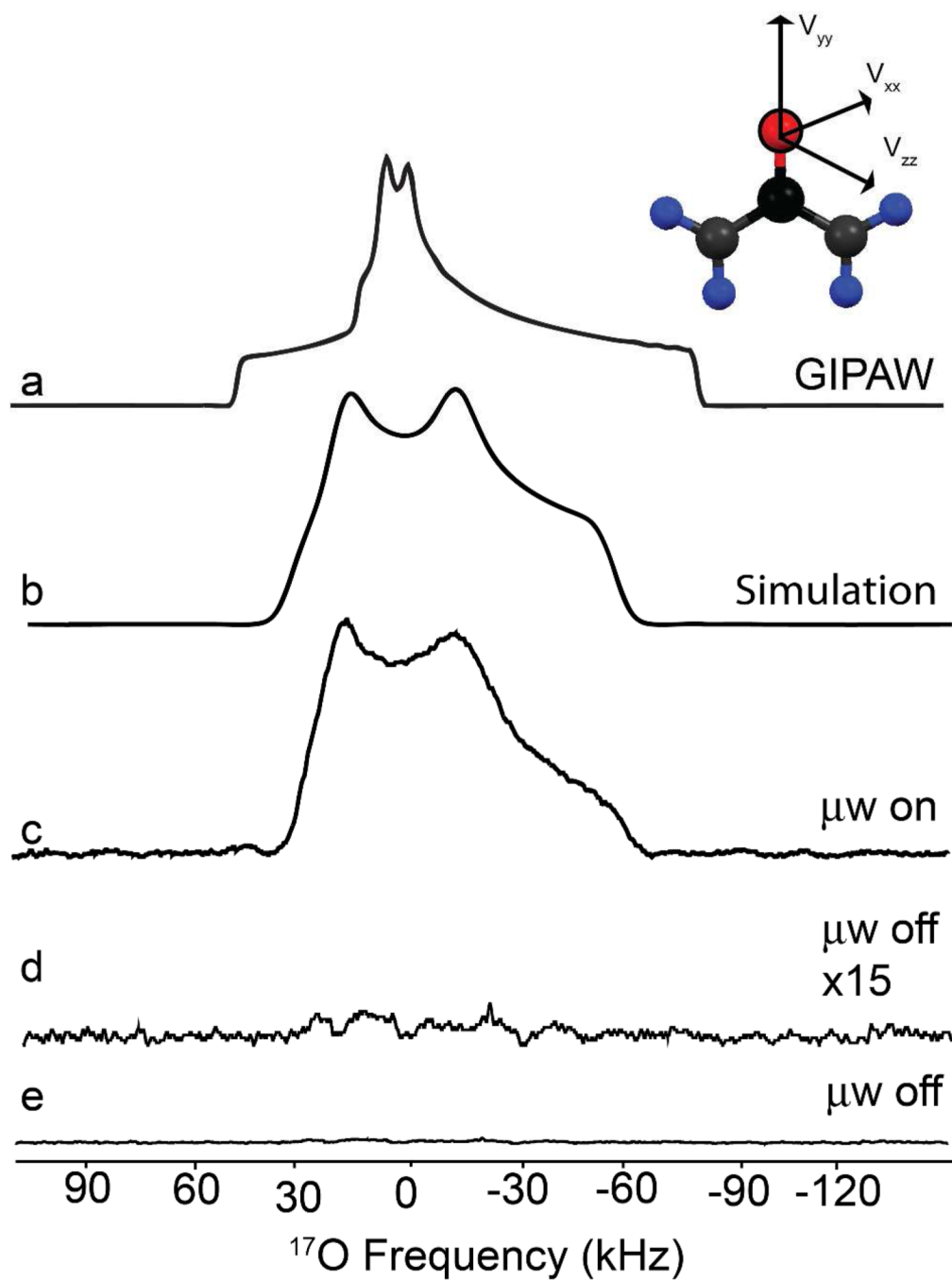


Figure 5. ^{17}O DNP NMR spectrum of ^{17}O labeled urea (4 mgs) in 60/30/10 (v/v) d_8 -glycerol/ D_2O / H_2O and 40 mM trityl using direct polarization. a) Simulation using GIPAW calculated parameters, b) simulation of quadrupolar lineshape, c) experiment on-signal (~ 8 hours), d) experiment off-signal scaled by 15 and e) experiment off-signal (~ 144 hours).

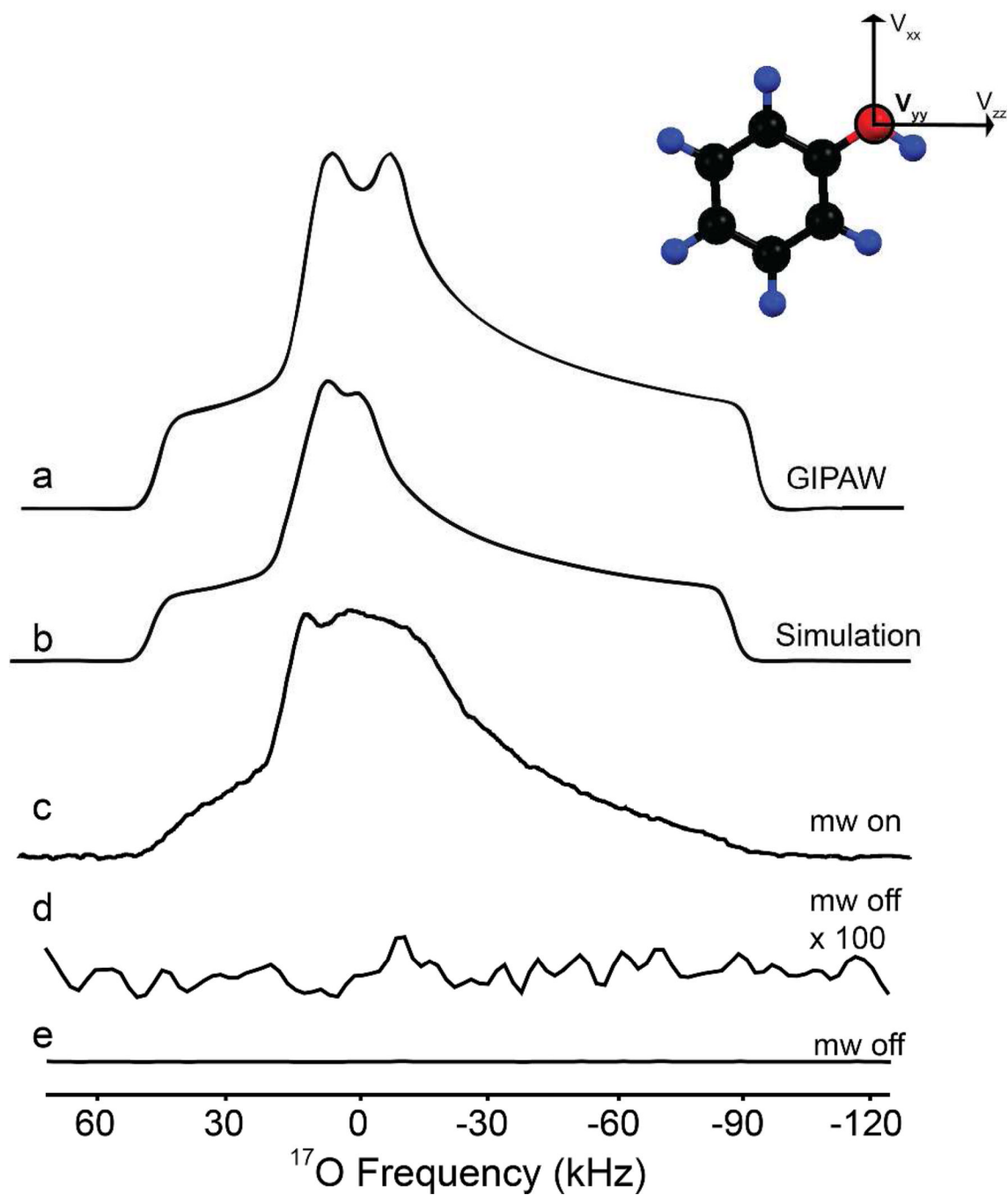


Figure 6. ^{17}O DNP NMR spectrum of ^{17}O labeled phenol (3 mgs) in 60/30/10 (v/v) d_8 -glycerol/ D_2O / H_2O and 40 mM trityl using direct polarization. a) Simulation using GIPAW calculated parameters, b) simulation of quadrupolar lineshape, c) experiment on-signal (~ 18 hours), d) experiment off-signal scaled by 100 and e) experiment off-signal (~ 144 hours).

Table 1

^{17}O enhancements and build-up times for direct polarization of oxygen in a 60/30/10 (v/v) d_8 -glycerol/ D_2O / H_2 ^{17}O (35%- ^{17}O - H_2O) with 40 mM electrons and sample temperature of 85 K.

<i>Radical</i>	<i>DNP Mechanism</i>	ϵ	T_{B} (s) ^c	$T_{1\text{s}}$ (ms)
SA-BDPA	SE	3 ± 0.6	5.2	28.9^{86}
TOTAPOL	CE	$7 (-8)^a \pm 1$	4.2	$\sim 0.3^{132}$
Trityl (OX063)	CE	115 ± 11	5.0	1.4^{86}
Mixture	CE	40 ± 6	5.7	$1.4/3.6^{b86}$

All enhancements were acquired at the field position of maximum positive value with and without microwaves.

(a) ^{17}O DNP enhancement for the biradical, TOTAPOL is non-symmetric, the value you parenthesis is the negative enhancement. The value in parentheses is the enhancement determined at the maximum negative point with and without microwaves.

(b) Values for trityl and SA-BDPA components, respectively.

(c) Nuclear spin-lattice relaxation times ($T_{1\text{I}}$) were measured independently (microwaves off) and found to be within experimental error to the DNP build-up relaxation times (T_{B}).

Table 2

Experimental (DNP and non-DNP) and calculated ^{17}O NMR parameters for model oxygen environments

Molecule	C_Q (MHz)	η	δ_{iso} (ppm)	Ω (ppm)	κ
Water (DNP)	6.8 (2)	0.95 (5)	0 (150)	n.d.	n.d.
Water (exp.) ⁱ	6.43	0.935	n.d.	n.d.	n.d.
Water (exp.) ⁱⁱ	6.66	0.935	0	n.d.	n.d.
Water (GIPAW) [*]	-6.833	0.90	-68.24	35.59	-0.40
Urea (DNP)	7.5 (3)	0.5 (2)	150 (150)	n.d.	n.d.
Urea (exp.) ⁱⁱⁱ	7.24	0.92	108	280	-0.857
Urea (GIPAW)	7.576	0.96	172.37	262.98	-0.82
Phenol (DNP)	8.3 (3)	0.95 (5)	100 (150)	n.d.	n.d.
Phenol (exp.) ^{iv}	8.3 (1)	0.95 (5)	80 (5)	n.d.	n.d.
Phenol (GIPAW) [*]	-8.686	0.84	81.61	71.12	0.53

ⁱ - Ba et al. 136;

ⁱⁱ - Spiess et al. 135;

ⁱⁱⁱ - Dong et al. 106;

^{iv} - ^{17}O MAS NMR data acquired at 17.4 T (see Figure S4);

^{*} - Where multiple crystallographic oxygen sites existed the averages of these are presented within the table (please refer to supporting information Tables S1 to S3). Experimental uncertainties are given in parenthesis. The Herzfeld-Berger¹⁴¹ convention is used to describe the chemical shift anisotropy, with the span (Ω) and skew (κ) defined as, $\Omega = (\delta_{11} - \delta_{33})$ and $\kappa = 3(\delta_{22} - \delta_{iso})/\Omega$, respectively.